Effect of micro- and nanoparticle shape on biological processes

Hicheme Hadji, Kawthar Bouchemal

Effect of Micro- and Nanoparticle Shape on Biological Processes

*Hicheme Hadji, Kawthar Bouchemal **

Université Paris-Saclay, Institut Galien Paris Saclay, CNRS UMR 8612, 92296, Châtenay-Malabry, France

Corresponding Author

* kawthar.bouchemal@universite-paris-saclay.fr

Abstract

In the drug delivery field, there is beyond doubt that the shape of micro- and nanoparticles (M&NPs) critically affects their biological fate. Herein, following an introduction describing recent technological advances for designing nonspherical M&NPs, we highlight the role of particle shape in cell capture, subcellular distribution, intracellular drug delivery, and cytotoxicity. Then, we discuss theoretical approaches for understanding the shape effect on particle internalization by the cell membrane. Subsequently, recent advances on shape-dependent behaviors of M&NPs in the systemic circulation are detailed. In particular, the interaction of M&NPs with blood proteins, biodistribution, and circulation under flow conditions are analyzed. Finally, the hurdles and future directions for developing nonspherical M&NPs are underscored.

Keywords: Nanoparticle; Shape; Cytotoxicity; Cell internalization; Biodistribution; Pharmacokinetics.

Contents

1. Introduction

Since the 60', micro- and nanoparticles (M&NPs) have had a powerful impact in biomedical applications such as imaging, diagnosis, and drug delivery. Since then, various classes of spherical M&NPs have been designed, mainly by tuning compositions, sizes, and surface properties. More recently, a new criterion to control biological processes has been added by conceiving M&NPs with specific shapes. Synthetic nonspherical M&NPs have been generated using different fabrication techniques divided into two categories: bottom-up and top-down approaches. Bottom-up fabrication relies on the association of specifically designed molecules into ordered structures. Chemical synthesis of particles with complex architectures (e.g., carbon nanotubes, inorganic particles) is based on bottom-up fabrication. Self-assembly of amphiphilic molecules constitutes the second group of bottom-up approaches. For example, disk liposomes[1] and filamentous micelles[2] were obtained by self-assembly processes. More recently, polymerization-induced self-assembly (PISA)[3, 4] offered the possibility to tune particle shape, size, and glass transition temperature[5] by varying the composition of starting materials during polymerization. A novel class of particles was recently designed by combining nonspherical particle shape to Janus properties.[6] Each particle face can be functionalized differently and independently.[6] In another embodiment, the self-assembly of hydrophobically modified polysaccharide and α-cyclodextrin in water resulted from hexagonal-shaped M&NPs, referred to as micro- and nanoplatelets.[7-14] It was possible to modify surface composition by changing the nature of the polysaccharide, while the size was adjusted by acting on the stirring duration of the starting materials.[12] Top-down approaches, on the other hand, are based on a controlled shaping of starting materials using different techniques such as lithography,[15-18] and physical stretching of spherical particles.[19-23]

All the available techniques have offered the possibility for a precise modification of particle shape, in addition to chemical, physicochemical, and physical properties. Consequently, the researchers considered particle shape as a novel parameter for controlling biological processes. Over the last decade, we have learned that particle shape mediates the motion in biological fluids in static conditions,[10, 24, 25] and under a shear flow,[26-30] interactions with the cell membrane,[31-34] endocytosis pathway,[18-21, 35-41] and intracellular distribution.[42-45] Herein, we will first review how M&NP shape impacts endocytosis. Both phagocytic and nonphagocytic pathways were underscored. Then, we will give a comprehensive analysis of whether particle shape impacts subcellular distribution and cytotoxicity. As an endocytosis process begins with the interaction of the particle with the cell membrane followed by the membrane deformation, a section will be dedicated to the multiscale

modeling of the mechanics and energies occurring during a wrapping episode. The complexity of the interaction between a particle and the cell membrane due to the shape effect will be discussed.

In this review, special attention was paid to the events occurring immediately after administering a particle in the body, even before interacting with the cell membrane. Immediately after their administration, the biomolecules present in the biological media (e.g., proteins, lipids, and sugars) will competitively bind to the M&NP surface leading to a biomolecular corona. Adsorption of blood proteins is most relevant since blood contains thousands of different proteins, each of which may potentially interact with a particle through non-covalent interactions.[46, 47] The protein corona controls pharmacokinetics, biodistribution, interaction with cells, intracellular trafficking, targeting capabilities,[48, 49] biological activity, immunological reactions,[50] and toxicity.[48] In this review, we will explore how nonspherical shape impacts particle behaviors in the systemic circulation, including interaction with blood protein, biodistribution, and circulation under a shear flow. We will analyze the possibility of manipulating the M&NP shape to escape the complement cascade's activation and prolong the circulation duration in the blood. Finally, we will discuss whether particle shape could dictate targeting a specific organ and increase therapeutic efficacy by encapsulating a drug.

2. Endocytosis

2.1. General overview

Endocytosis is a general term describing a fundamental cellular process by which the eukaryotic cells internalize substances from the extracellular environment. The substances to be engulfed are surrounded by pieces of the cell membrane and carried into the cell in vesicular structures that eventually pinch off the membrane inside the cell (Figure 1). Endocytosis plays a critical role in nutrient uptake, surface receptor regulation, cell motility, cell adhesion and orchestrates several cell signalling pathways. Viruses and bacteria exploit this process to enter the cells.

Endocytosis is usually subdivided into two internalization mechanisms: ‘phagocytosis’ or cell eating and ‘pinocytosis’ or cell drinking. Pinocytosis is also referred to as a nonphagocytic pathway. Phagocytosis is mainly undertaken by professional phagocytes of the immune system, including neutrophils, macrophages, and mature dendritic cells.[51] In addition to professional phagocytes, the engulfment of cells by nonprofessional phagocytic cells has been described for decades. In this process, living cells engulf other living or dying cells. High rates of nonprofessional phagocytic pathways were reported in cancer cells. This phenomenon was called cell cannibalism,[52, 53] which is defined as ‘a cell that is contained within another bigger cell with a crescent-shaped nucleus’.

Pinocytosis occurs in all cells according to four main engulfment mechanisms depending on the different proteins and lipids involved: macropinocytosis, clathrin-mediated endocytosis, caveolae-mediated endocytosis, and clathrin- and caveolae-independent endocytosis. Clathrin-mediated endocytosis is the most elucidated mechanism for nonphagocytic pathways of M&NPs and macromolecules. Unlike phagocytosis, all mammalian cells can ensure this uptake pathway,[54] which mainly engages receptor-ligand complexes. Endocytic coat proteins in the cytosol start to cluster on the inner plasma membrane upon binding of a ligand to its receptor on the cell membrane. The process continues with further recruitment of coat proteins from the cytosol. The process involves a triskelion-shaped protein called clathrin. The flat membrane transforms on a 'clathrin-coated pit' following the self-organization of clathrin into cage-like structures (Figure 1). Subsequently, the pit becomes deeper until it pinches inside the cytoplasm as vesicles (120 nm size) that are typically delivered to the early endosomes (See Transmission electron microscopy (TEM) images in Figure 2). (For review on clathrin-mediated endocytosis pathway see[54])

Caveolae-mediated endocytosis is a clathrin-independent endocytosis pathway. It is present in different cells, mainly endothelial cells. Over this internalization process, a dimeric protein called caveolin triggers the invagination of the cell membrane in the cytosolic side and forms small flask-shaped caveolae ($50-60$ nm) (Figures 1 and 2). Then, the cargo containing caveolar vesicle is detached from the cell membrane and released into the cytosol after a GTPase dynamin ensures the fission from the cell membrane. Although this endocytic pathway is described to be relatively slow (half-time >20 min), the internalized materials could bypass the endosomal and/or the lysosomal compartments.[55]

Macropinocytosis, also called big drink, is clathrin- and caveolin-independent endocytosis pathway. It occurs in most mammalian cells, including professional phagocytes[56] and cancer cells under stimuli such as growth hormones.[57] Macropinocytosis is mostly initiated by actin-driven membrane ruffles (Figures 1 and 2). These laters often fuse with the cell membrane to form large vesicles (macropinosomes), whose size varies from 0.2 µm to more than 5 µm (Figure 1). For review, see reference[58]. Once inside the cytoplasmic environment, unmatured macropinosomes shrink through a series of tubulations and fissions.[59] Then, they sequentially fuse with endosomes and lysosomes.

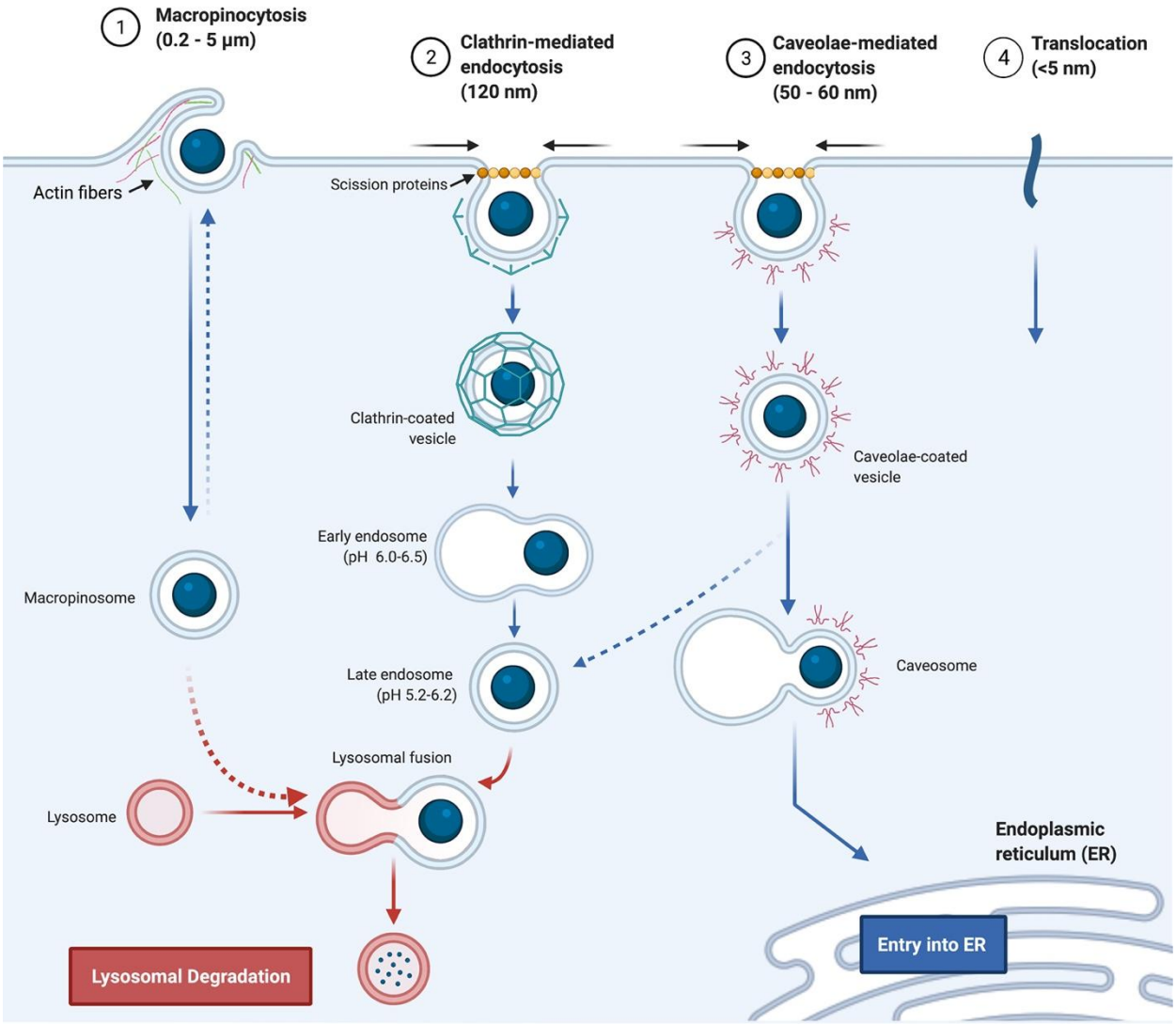

Figure 1: (A) Illustration of the main nonphagocytic pathways in eukaryotic cells.

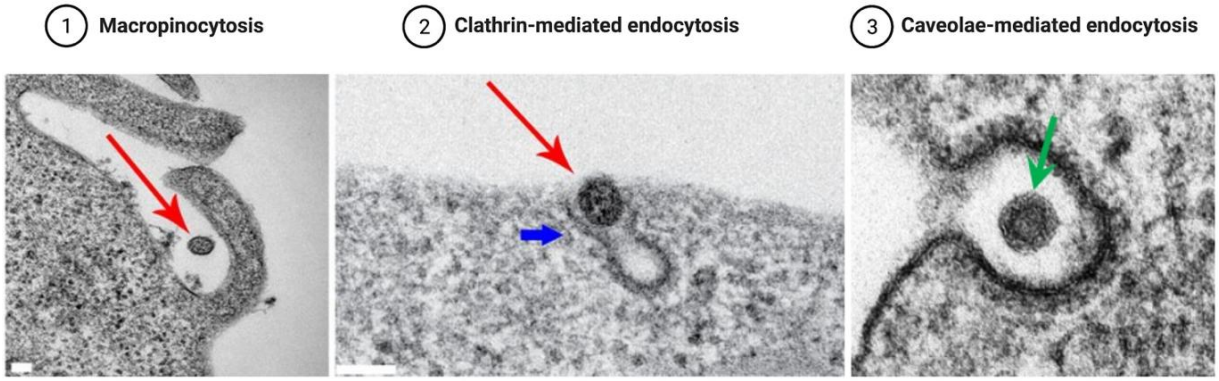

Figure 2: Transmission electron microscopy images of micropinocytosis (1), clathrin-mediated endocytosis (2) (Reproduced from reference[60] with permission), and caveolin-mediated endocytosis (3) (Reproduced from reference[61] with permission). In (1) and (2), the red arrows indicate filamentous influenza virion undergoing clathrin-mediated endocytosis. The blue arrowhead in (2) indicates the clathrin lattice. Scale bars in (1) and (2) correspond to 100 nm. The image in (3) represents the entry of Simian Hemorrhagic Fever Virus (green arrow) into MA-104 cells through caveolin-mediated endocytosis at 5 min. Noteworthy, the image published in reference[61] without scale bar, but the diameter of ranges from 40 to 50 nm.

2.2. Shape-dependent endocytosis

While it is beyond doubt that particle size and surface properties significantly impact their cellular internalization pathway, shape-dependent cell uptake has been studied more recently. Investigating the impact of particle shape on phagocytosis determines whether undesirable capture by the mononuclear phagocytic system (MPS) can be limited. In contrast, the cell capture of M&NPs can dictate therapeutic applications for intracellular drug delivery. The mechanism by which the M&NPs are captured dictates intracellular transport and the possibility to target specific intracellular compartments by acting on particle shape, as detailed in section 2.3. Although there is evidence that M&NP shape affects the rate and the mechanism of particle endocytosis,[18, 62-67] contradictory data were reported on the shape-dependency of M&NPs cellular uptake. Previous works showed that the shape of M&NPs affects phagocytosis,[21] internalization by nonphagocytic cells,[18] and intracellular transport.[63] In contrast, other works reported that M&NP geometry does not play a dominant role in their cellular uptake.[68] Hereafter, the influence of M&NPs shape on cellular uptake was analyzed and discussed.

2.2.1. Phagocytosis of nonspherical particles

The phagocytosis process is critical in eliminating invading pathogens such as viruses, bacteria, yeasts, and dead cells.[69] It is also involved in immune regulation, inflammation, and cancer. In the drug delivery context, the phagocytic mechanism was extensively studied for exogenous M&NPs as it regulates their biological fate and toxicological behaviors.[70] One crucial step before particle phagocytosis is their opsonization. This process consists of attaching proteins, called opsonins, on

the surface of the particles to be engulfed. Opsonized particles are thus tagged and will be recognized by the phagocyte membrane receptors. To date, several opsonins have been reported, including complement components,[71] immunoglobulins (e.g., IgM, IgG), type one collagen, and C-reactive protein.[72] Conventional receptors for opsonized particles include the Fc region of immunoglobulins, complement receptors, and scavenger receptors.[73] Others investigated the effect of other receptors such as CD44 in the opsonization process.[74] Importantly, unopsonized particles can also be recognized by phagocytes, either as a consequence of the presence of specific patterns in their surface such as carbohydrates residues (Mannose, I-fructose, glucose) or via the CD11/CD18 integrins receptors that can bind to both opsonized and unopsonized particles.[75]

Once introduced to the phagocyte's membrane receptors, a signalling cascade will trigger the assembly of actin.[76] This event provides a force necessary for forming cell membrane extensions that engulf the foreign particle and create a phagosome,[77] (Figure 3.A) which will carry the uptaken particles in the cytoplasm. After actin depolymerization, the phagosome transforms into an intracellular vacuole membrane. This later fuses with the endosomes and eventually lysosomes forming phagolysosomes,[78] which acidic environment is responsible for the engulfed particle's degradation.[79]

Although M&NP uptake by macrophages is usually undesirable, it was also exploited to target reticuloendothelial system for the delivery of drugs (e.g., cytotoxic, antiparasitic, antifungal, antibacterial, antiviral, and anti-inflammatory drugs). In the drug delivery context, the impact of M&NPs size and surface chemistry on phagocytosis was investigated by several research groups. Studies have suggested that macrophage phagocytes can engulf a wide range of particle sizes from 250 nm to several micrometers.[53, 80] It is also known that macrophage phagocytes can *'*eat bigger than their head*'*.[81] The engulfment of large particles is essential for host defense against infection and removing dead cells.

Along with the size, the shape of M&NPs has emerged as a critical attribute of their internalization by macrophages. The Mitragotri group revealed that particle shape plays a crucial role in macrophage phagocytosis.[20, 21, 35, 36] Polystyrene particles were prepared by the film stretching method. They had variables sizes and shapes: spheres (radius varied from 1 to 12.5 μm), oblate ellipsoids (1×4 μm, AR 4), prolate ellipsoids (major axis $2 - 6$ μm, AR $1.3 - 3$), elliptical disks (major axis $4 - 8$ μm, AR $1.5 - 4.5$) and UFO-shaped particles (sphere radius 1.5 μm, ring radius 4 μm).[21] Particle internalization revealed that the phagocytosis kinetic was controlled by the local geometry of the particle-cell interface. In this regard, ellipsoidal disks (3×14 μm) were internalized

within a few minutes (< 6 min) when the tangent angle (Ω) of the particle surface with macrophages was smaller than 45° (Figure 3.A). In contrast, for Ω > 45° (Figure 3.B), the macrophages, attached to the flat side of the particle, were able to spread on the particle surface but did not internalize it even after 12 h.[21] Importantly, those results were related to the differences in the actin structure formed when the particle interacted with the macrophage surface. Indeed, when the particle was attached to the cell with its flat side, actin polymerized at points of contact but failed to create the adequate actin structure necessary to engulf the particle (Figure 3.B).

Those findings could be interesting for different applications, including the possibility of acting on particle shape to inhibit particle phagocytosis by macrophages.[82] It was demonstrated that worm-like particles with high AR (> 20) exhibited negligible phagocytosis compared to spherical particles with equivalent volume.[82] Videomicroscopy and fluorescence microscopy techniques revealed that worm-like microparticles interacted with macrophages at the two-particle endpoints (Figure 3.C).

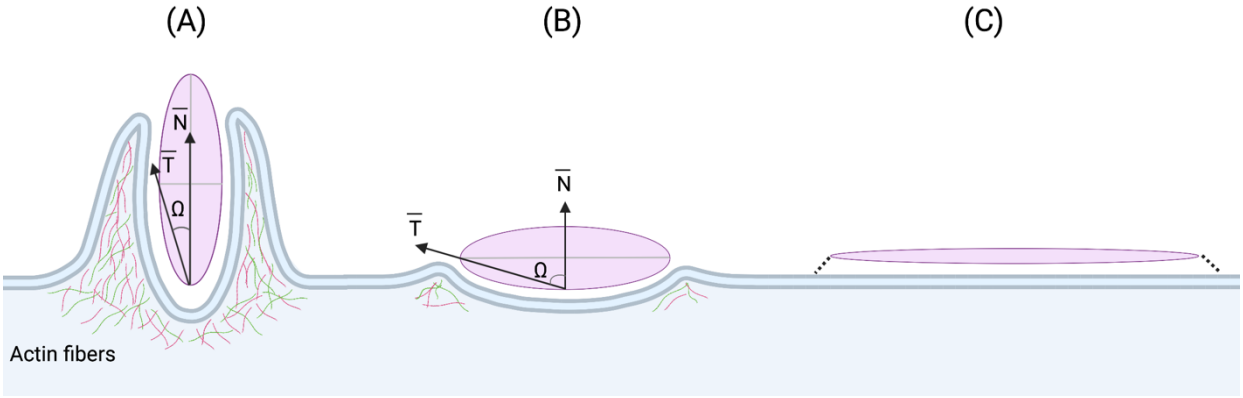

Figure 3: Schematic representation of the different orientations of a particle during phagocytosis. The tangent angle Ω between $\overline{N}$ and $\overline{T}$ was < 90° in (A) and > 90° in (B). Dash lines in (C) represent the interaction of high AR particles at the two-particle endpoints. Adapted with permission. from references.[21, 82]

2.2.2. Nonphagocytic pathways of nonspherical particles

2.2.2.1. Improved cell uptake of nonspherical particles

Several studies suggested that nonspherical M&NPs were taken up by cells at faster rates and in more significant amounts than spheres. Comparing the cellular uptake of mesoporous silica M&NPs with different aspect ratios (Ars) showed that particles having larger ARs were taken up by cells (e.g., HeLa cells, human melanoma cells, and adenocarcinomic human alveolar basal epithelial cells) in large amounts and had faster internalization rates.[66, 67] The particles had similar equivalent diameter, surface composition, and surface charge but different AR: nanospheres (AR of ~1, diameter ~100 nm), short rods (AR of ~2 and ~240 nm in length), and long rods (AR of ~4 and 450 nm in length).[66] The number of long rods internalized by cells was almost twice that of short rods.

Similar results were reported earlier by Gratton and coworkers.[18] In this investigation, hydrogel particles with variable size, shape, and surface charge were designed by a top-down lithographic fabrication method called PRINT™ (Particle Replication In Nonwetting Templates).[83, 84] While all the particles were internalized by HeLa cells, high AR cylindrical particles (150×450 nm) were internalized faster than cubic particles and short cylinders. Those cylindrical particles had an AR of 3 and were taken up by cells ~4 times faster than spheres. The particles were positively charged and had a similar volume.

In agreement with those findings, other investigations showed that rod-like polymeric micelles were taken up by Caco-2 cells 12 times more efficiently than spherical particles with similar compositions.[85] The exact mechanism for faster and higher internalization rates of nonspherical M&NPs is not well elucidated. However, the increased surface area of a long rod and disk particles with the cell membrane is believed to play a relevant role in cell internalization.[18, 19, 37-39]

In addition to AR, the sharpness of the edges was found to be a relevant parameter for cell internalization. For instance, it was found that microparticles that had sharp edges were faster internalized by cells than round-shaped particles.[40] While the exact mechanism was not yet studied; the authors explained those differences by the possible difficulty to recruit enough actin filaments for round-shaped particles compared to particles with sharp edges.[40] Similarly, Hu et al.,[41] revealed that particles with irregular spiked surfaces exhibited faster cellular uptake than spheres and smooth disks. The shape-controlled nanostructures were formed by the hierarchical self-assembly approach of amphiphilic block copolymers.

2.2.2.2. Decreased cell uptake of nonspherical particles

Several studies suggested that cellular internalization of nonspherical M&NPs through nonphagocytic pathways was reduced compared to spherical particles. In particular, Au nanospheres were taken up by cells to a larger extent than chemically similar nanorods.[65] In this experiment, uptake efficiency was inversely proportional to AR. The cellular internalization of Au nonspherical particles tends to be reduced compared to spherical particles. [65, 86] However, it is worth noting that the surface properties of spherical and rod-like M&NPs are different. Indeed, the surface of the Au spherical particles is coated with citric acid, while the nanorod surface was stabilized with cetyl trimethylammonium bromide (CTAB). The differences in surface composition of rods and spheres may partially explain the contradictory results obtained with other particles.

Nevertheless, similar trends were also reported for polystyrene disk particles.[19, 38] Indeed, while spherical particles enter the cells and perturb the cellular function, the disks bind only to the cell

membrane with a significantly reduced cellular function such as reactive oxygen species (ROS) generation, apoptosis, and cell cycle progression.[38] The nanospheres and the disks had similar diameters ($\sim$20 nm) and surface potentials ($\zeta \approx -24$ mV in serum). As the disks had a 2 nm thickness, the volume was not constant. Furthermore, the nanoparticles used in this investigation are about 10 to 50 times smaller than those used in further experiments revealing preferential cell uptake for nonspherical particles.

Lower cell uptake for nonspherical M&NPs agrees with theoretical models based on free energy minimization. In a model developed by Decuzzi and Ferrari,[64] it was predicted that nanoparticles with extremely low or high AR were not endocytosed. The AR should be in an intermediate range for complete wrapping by the cell membrane.

2.3. Subcellular distribution

We have detailed how the M&NPs interact with cells and how they are internalized depending on their shape. While the correlation between the M&NP shape, their interactions with cells, and the internalization mechanism has been thoroughly investigated, only a few studies addressed their distribution inside the cells. Beyond the internalization mechanism, understanding the intracellular distribution of M&NPs is essential for the subcellular drug delivery to the target compartment, cell imaging, and understanding cytotoxicity behaviors. The intracellular distribution of a drug or its carrier is mediated by the internalization route (Figure 1). After their cell uptake, most M&NPs are confined in early endosomes, which would mature into late endosomes and then lysosomes before exocytosis.[87] Several strategies have been envisioned for endosome targeting through receptor-mediated internalization. Ligands such as folate, transferrin, and low-density lipoproteins have been exploited for their ability to bind receptors that are overexpressed in malignant tumors for therapy or imaging.[88, 89] The pH of early endosome ($\sim 6 - 6.5$) was exploited to design pH-sensitive delivery systems to treat severe diseases such as cancer or Alzheimer's disease.[90, 91] However, the internalization of the early endosome could represent a hurdle in developing M&NPs for targeting other subcellular compartments such as the cytosol or the nucleus. Most of the drug-loaded particles that are endocytosed accumulate in late endosomes and lysosomes, where they are degraded due to harsh acidic pH or removed from the cell before reaching the target subcellular compartment (Figure 1).[92] For example, mRNA or siRNA carriers must escape the endosome to be released into the cytosol, where they interact with the RNA machinery. To release the drugs in the cytosol and avoid endosomal degradation, ionizable lipids were used in designing lipid-based nanoparticles. These lipids are neutral at physiological pH but protonated in endosomes. In this way, lipid ionization

facilitates the fusion of their lipids with the endosomal membrane and enables cytosolic RNA delivery (For reviews on mRNA delivery, see references [93, 94]). In another embodiment, it was demonstrated that particles with sharp corners and edges offered a rapid endosomal escape to the cytosol by breaking the endosome's membrane.[42, 43] Soft-shaped particles failed to escape the endosome, regardless of their surface charge, size, and composition. The AR of the particles used in this study was ~ 1, the average size was ~ 115 nm, and most of the particles had at least 1 or 2 sharp corners.[42]

Shape-directed subcellular compartmentalization was already demonstrated with iron oxide nanoparticles.[44] The particles had similar composition and surface charge but differed by their shape (spheres, spindles, biconcave particles, and nanotubes). The intracellular distribution revealed that the biconcave particles were preferably localized in the nucleus, whereas spheres were distributed in the cytoplasm and nucleus. The spindle and nanotube geometries were observed mainly in the cytoplasm. In another investigation, Xu et al.,[45] revealed that layered double hydroxide nanorods ($30-60$ nm in width and $100-200$ nm in length) and nanosheets ($10-20$ nm in thickness and $50-150$ nm in lateral wide) were internalized through clathrin-mediated endocytosis, and they rapidly escape the endosome. The authors revealed that the intracellular distribution is shape-dependent since the nanorods quickly translocated into the nucleus while nanosheets were retained in the cytoplasm. The authors hypothesized that the width of layered double hydroxide nanorods reduced from $30-60$ nm to $20-30$ nm after deacidification within the endosome. Indeed, layered double hydroxides are a family of anionic materials that can buffer endosome acidification. Consequently, protons were pumped from the cytosol, leading to particles releasing into the cytosol. Considering that the cylindrical nuclear pores are $20-30$ nm in width, it is likely that the nanorods enter the nucleus after the endosomal escape. The size-fit of short single-walled carbon nanotubes (SWNTs) to the nuclear pores partly explained their rapid translocation into the nucleus. SWNTs, characterized by a diameter of ~ 1 nm and a length of $\sim 300-1000$ nm, could cross the lipidic cell membrane through an energy-dependent nonendocytic pathway (Figure 1.4) and mainly distributes inside the nucleus.[95] While others suggested that energy-dependent endocytosis pathways may occur for SWNTs. For example, SWNTs ($\sim 50-200$ nm in length) were internalized by cells primarily by a clathrin-coated pit pathway.[96] While there is no doubt on the cell internalization and accumulation of SWNTs in the nucleus, a central question is whether those particles are excreted from the cells by exocytosis. Jin et al.,[97] studied SWNT exocytosis by using single-particle tracking. The exocytosis rate closely matched the endocytosis rate.

From another perspective, several studies revealed that the shape and AR of M&NPs dictated the cell internalization mechanisms and significantly impacted intracellular trafficking (Table 1). Macropinocytosis and clathrin-mediated endocytosis were the main mechanisms for cell entry of ellipsoidal polymeric particles.[98] The ellipsoids were formed by the nanoprecipitation of poly(glycerol sebacate)-*co*-polyethylene glycol (PGS-*co*-PEG) copolymers. The dimensions of the ellipsoids were changed by acting on the molar ratio of PEG within the copolymer: AR ~4.9 (235 × 48 nm) or AR ~2.4 (195 × 80 nm).

In other investigations, the uptake of rod-shaped mesoporous particles with an AR of $2.1-2.5$ ($60-90 \times 160-190$ nm) was internalized through a macropinocytosis process.[67] The particles with an intermediate AR were endocytosed faster and in a higher amount than particles with low AR (1~1.2) and high AR (4.0~4.5). Interestingly the rod particles with an intermediate AR accumulated preferentially in the perinuclear region, while shorter and longer rods were more randomly distributed in the cell. Gratton et al., [18] revealed that hydrogel PRINT^{TM} nanoparticles with an AR of 3 (150×450 nm) were rapidly internalized into cells and translocated close to the nuclear membrane. Those particles were internalized by cells through multiple modes of non-specific endocytosis, most notably by a clathrin-mediated mechanism, caveolae-mediated endocytosis, and to a lesser extent, macropinocytosis.

However, other findings revealed that nanoparticle shape and AR did not significantly affect intracellular trafficking. The impact of Au nanoparticle shape on intracellular trafficking was investigated by varying the ARs from 1 to 7.[99] Both spherical and rod particles were functionalized with DNA oligonucleotides to target class A scavenger receptors. The particles entered the cells through a caveolae-mediated pathway regardless of the AR. Targeted nanorods reached the late endosome within 4 to 8 h post-incubation with cells, but they did not progress from the late endosome to the lysosome. In agreement with these findings, the lysosomal compartmentalization was independent of the shape of soft hydrogel capsules.[100] In this investigation, the AR varied from 1 to 3.8. Shi et al.,[101] reported a higher accumulation of rod-like particles with high AR (~ 18×102 nm) in the endosome and the lysosome than low AR rods (~25×74 nm). Intracellular trafficking experiments were performed on polyplexes of *N*-(2-hydroxypropyl) methacrylamide-oligolysine brush polymers. When both polyplexes had the same molecular weight and chemical composition, they differed in the oligolysine length, which confers to them a different shape. Furthermore, the preferential accumulation of high AR rod-like particles in the endosomal/lysosomal compartments delayed nuclear delivery. Those findings were attributed to the cationic polyplexes

that could interact through multivalent interactions with the endosomal and lysosomal membranes. Higher interactions are expected with a higher surface area offered by rod-shaped polyplexes.

Table 1: Summary of the effect of the M&NP shape on the cell internalization pathway.

Particle type	Shape	Endocytic pathway	Methods for characterizing particle cell uptake	Dimensions (nm)	ζ (mV)	Cell line	Ref
Hydroxyapatite crystals	Plates	Macropinocytosis	CLSM	221 × 115	-8.45	A7R5[a]	[102]
	Spheres	Clathrin-mediated endocytosis		63 × 63	-2.57		
	Needles	Multiple pathways		227 × 44	-4.58		
	Rods	Mainly macropinocytosis followed by caveola-mediated endocytosis		129 × 41	-7.02		
Mannose-functionalized micelles[#]	Spheres	Clathrin- and caveola-mediated endocytosis	CLSM, flow cytometry	46 × 46	-10.9	RAW 264.7[b]	[103]
	Short cylinders	Clathrin-mediated endocytosis		99 × 50	-13.9		
	Long cylinders	Clathrin-mediated endocytosis		215 × 47	-13.3		
Silica M&NPs	spheres	Clathrin-mediated endocytosis	CLSM, TEM	178 × 178	87	A549[c] & RAW 264.7[b]	[68, 104]
	worms	Macropinocytosis		232 × 1348	58		
Au nanoparticles	Stars	Clathrin-mediated endocytosis	ICP-AES, TEM	~68.55	-2.47	RAW 264.7[b]	[105]
	Rods	Clathrin- and caveolae-mediated endocytosis		~70.49	40.53		
	Triangles	Clathrin Dynamin dependent pathway		~61.33	36.07		
Au nanoparticles	Stars	Clathrin and Caveolae	ICP-AES, TEM, dark field microscopy	15 × 15	-13.87	SMMC 7721[d] & GES-1[e] & 4T1[f]	[106]
	Rods	Clathrin		33 × 10	54.27		
	Sphere (small)	Clathrin		15 × 15	-25.8		
	Sphere (medium)	Clathrin		45 × 45	-25.4		
	Sphere (large)	Macropinocytosis		80 × 80	-8.83		
Silica particles	rod	Macropinocytosis	Flow cytometry, CLSM, TEM	60-90 × 160-190	13.0	HeLa	[67]

a/ aortic smooth muscle cell line, b/ macrophages, c/ human lung tumor epithelial cells, d/ human hepatocarcinoma cell line, e/ human gastric epithelial cell line, f/ mouse breast cancer cell line. [#]two different polymers were used for the nanoparticle design: poly(DL-lactic acid)-*b*-poly-(acrylic acid) for spherical micelles and poly(L-lactic acid)-*b*-poly(acrylic acid) for cylindrical micelles. CLSM: Confocal laser scanning microscopy. TEM: Transmission electron microscopy. AFM: Atomic force microscopy. IPC-AES: Inductively coupled plasma-atomic emission spectrometer.

2.4. Intracellular drug delivery

A key question is how to exploit shape-dependent cell uptake for efficient drug delivery? In this regard, it was demonstrated that rod-shaped mesoporous silica particles with an AR of $\sim 2.1 - 2.5$ were more efficient in delivering hydrophobic chemotherapeutic agents (e.g., camptothecin or paclitaxel) than spherical ones.[67] The cytotoxic potential of the encapsulated drugs was studied in HeLa cells. In a study conducted by Enlow et al.,[15] cylindrical poly(lactic acid-*co*-glycolic acid) (PLGA) particles (200×200 nm) prepared by PRINT^{TM} process showed high and efficient loading of docetaxel. Particles containing up to 40 wt% of the drug showed higher cytotoxicity than Taxotere. Similarly, the cell uptake and the cytotoxicity of tubular polymersome-loaded doxorubicin were higher than for spherical particles.[107]

Nonspherical M&NPs showed promising results for the intracellular delivery of nucleic acids, which is challenging because of their negative charge and degradation in physiological conditions. For instance, SWNT/DNA complexes resulted in an efficient gene delivery capacity in cells.[108] SWNTs had a diameter of 20 nm and a length of 200 nm. In another investigation, small interfering RNA (si-RNA)-encapsulated needle-shaped PLGA particles (80×320 nm) were generated by PRINT^{TM} process.[109] Particle surface was coated with lipids DOTAP:DOPE ($1:1$ wt%) to increase the transfection efficiency (DOTAP: 1,2-dioleoyl-3-trimethylammoniumpropane, DOPE: dioleoylphosphatidylethanolamine). The particles were efficiently internalized by different cell lines, and the knockdown of therapeutically relevant genes was demonstrated.[109] In a more recent investigation,[110] the si-RNA loading, release and internalization efficiencies, and effectiveness of post-transcriptional gene silencing of hollow Au particles ($45 - 50$ nm size) with different shapes and dimensions were compared (nanoshells, nanocages, and nanorods). The three particles were internalized by cells, but nanoshells and nanocages displayed the highest knockdown efficiency.

2.5. Cytotoxicity

Among the different available approaches to evaluate the safety of M&NPs, in vitro experiments represent the first step before selecting the most promising preparation to be tested ex vivo and in vivo. A panel of cell viability tests is available to evaluate cytotoxicity, as summarized in Table 2. Compared with M&NPs size and surface properties, the effect of particle shape on cytotoxicity was more recently studied. Efforts devoted to understand the relationship between particle shape and cell toxicity highlighted contradictory results (Table 3). For example, no significant cytotoxicity was observed with cylindrical PEGylated PRINT^{TM} microparticles after 4 h or 72 h of incubation with four different cell lines, including HeLa and macrophages.[16] The microparticles had a mean height of

0.68 μm, a mean width of 1 μm, and positive or negative zeta potentials. In another investigation, PEGylated nanoimprinted disks ($325\ nm \times 100\ nm$), and rod-shaped particles ($400\ nm \times 100\ nm \times 100\ nm$) did not induce cell death on three different cell lines (HeLa, HEK 293, and HUVEC). A ratio of 10^5 particles per cell was used.[39] As expected from the biocompatible and biodegradable PLGA, M&NPs were not toxic on cells regardless of their shape.[15] In this investigation, cylinders (200 nm × 200 nm, 320 nm × 80 nm, or 600 nm × 200 nm), 2 μm cubes, and 3 μm particles with center fenestrations were tested on ovarian carcinoma cells. In agreement with those findings, ellipsoidal particles composed of PGS-*co*-PEG copolymers with two different AR (AR ~4.9, 235 nm × 48 nm and AR ~2.4, 195 nm × 80 nm) did not show any toxicity toward two cell lines preosteoblasts.[98] Similarly, changing the shape from spherical to rods, cylinders, disks, or worms of silica, Au, or polystyrene nanoparticles did not affect cell viability.[38, 68, 86, 104, 111, 112] Collectively, it was found that the cytotoxicity was rather related to particle concentration, surface charge,[109] particle size, and the cell type.

In opposition to these results, other studies showed that AR had a significant impact on cell death. The cytotoxicity of high AR silica nanorods (AR ~4, 450 nm in length) was higher than low AR nanorods (AR ~2, 240 nm in length).[66] It was found that DNA-coated Au nanorods that had high AR (~4 or 7) induced higher cytotoxicity than low AR nanorods.[99] Similarly, nanorods and star-shaped particles had higher toxicity compared to spherical particles.[106] In another investigation, both diameter and AR of cerium oxide nanorods were varied to determine the critical AR that induced cell death.[113] The AR varied from 1 to > 100 (from 33 to > 1000 nm in length and 7 to 9.5 nm in diameter). While no significant cell death was reported with low AR nanorods (up to 31), the highest AR induced significantly higher cell death and activated the NALP3 inflammasome. Subsequent activation of the multiprotein complex NALP3 inflammasome activates caspase 1, leading to pro-inflammatory cytokines including interleukin-1β (IL-1β) and IL-18. For review, see reference[114]. Similar conclusions were drawn for high AR multi-walled carbon nanotubes, which activated NALP3 inflammasome and led to cytokine release in a human monomyelocytic leukemia cell line.[115] Some researchers showed that the cytotoxicity of multi-walled carbon nanotubes could be decreased by acting on their length.[116, 117] Indeed, short carbon nanotubes (600 nm in length) induced less ROS and inflammatory cytokines than long nanotubes (20 μm in length). Several studies showed that long (> 15 μm in length) and more rigid multi-walled carbon tubes were not wrapped by macrophages. Frustrated phagocytosis in macrophages induced chronic granulomatous inflammation due to the release of reactive oxygen species and hydrolytic enzymes.[118, 119] Interestingly, spherically shaped carbon nanotubes induced lower cytotoxicity than high AR multi-walled carbon nanotubes.[120] In a

recent study, Nahle et al.,[121] studied the effect of the morphology of carbon nanotubes on their cytotoxicity on rat alveolar macrophage cell line. Their results showed higher toxicity of multi-walled carbon nanotubes than single-walled carbon nanotubes.[108] The nanotubes were ammonium functionalized and had a diameter of about 20 nm and an apparent length of about 200 nm. In addition to the shape and the length, other characteristics could contribute to adverse biological outcomes, including surface functionalization. Indeed, significant differences in cytotoxic behaviors were observed with multi-walled carbon nanotubes ($10-30\,\mu m$ in length and $20-30\,nm$ in diameter), which induced less profibrogenic effects when functionalized with carboxylic groups.[115]

Table 2: Commonly used methods and assays to determine M&NPs cytotoxicity.

Toxicity test	Principle	Data interpretation	Ref
MTT assay	MTT is a colorimetric assay, which determines the mitochondrial activity in living cells. It is based on the reduction of MTT (3-[4,5-dimethylthiazol-2-yl]-2,5-diphenyl tetrazolium bromide) (yellow colored) by the action of mitochondrial oxidoreductase enzymes. This reduction results in insoluble purple formazan crystals that can be quantified after solubilization in dimethyl sulfoxide and measuring the optical density at 570 nm.	The purple color's intensity (or optical density) is directly proportional to the mitochondrial oxidoreductase activity. The healthy cells exhibit high rates of MTT reduction to formazan and high optical density, corresponding to lower cytotoxicity of the M&NPs at the tested concentration.	122, 123
MTS assay	MTS is a colorimetric assay based in the reduction of the MTS reagent (3-[4,5-dimethylthiazol-2-yl]-5-(3-carboxymethoxyphenyl)-2-(4-sulfophenyl)-2H-tetrazolium). In MTS assay, the formazan dye is soluble in cell culture media, and the optical density is measured at 490-500 nm.	Similar to MTT assay, the purple's color intensity is correlated to the cell viability. Lower optical density corresponds to higher cell death.	124, 125
LDH assay (or LDH release assay)	In the lactate dehydrogenase (LDH) assay, the level of plasma membrane damage in a cell population is assessed. LDH is an enzyme found in the cytoplasm of living cells. When the cell membrane is damaged, the LDH is released into the cell culture medium. The assay is based on the reduction of tetrazolium salt into a red-colored formazan dye. The optical density is measured at 492 nm.	The cell death is proportional to the intensity of the red color, which is proportional to the reduction of tetrazolium salt by the LDH leaked into the cell culture.	123, 126 127
ROS assays	Reactive oxygen species are produced inside the cells as a response to environmental stress. There are several assays for the detection of ROS: - Fluorescence dependent methods - Chemiluminescence dependent methods - Spectrometry methods - Chromatography methods - Electrochemical biosensors - Electron spin resonance - Fluorescent protein-based methods.	Elevated ROS (e.g., elevated intensity in the fluorescence or spectrometry methods) is highly correlated with cell death by necrosis or apoptosis.	127 128
WST-1® assay	WST-1 (2-(4-iodophenyl)-3-(4-nitrophenyl)-5-(2,4-disulfophenyl)-2H-tetrazolium) is a water-soluble reagent. It does not penetrate the cell but is instead cleaved by the succinate-tetrazolium reductase at the cell surface to form a water-soluble formazan dye. The optical density of formazan dye is measured at 450 nm.	Similar to MTT and MTS assays, the cell viability is correlated to the optical density intensity.	129
WST-8® assay (CCK-8® assay)	WST-8® (CCK-8®) assay is based on the same principle as WST-1® or MTS assay but exhibits superior detection sensitivity by the tetrazolium salts are highly soluble. The optical density of formazan dye is measured at 450 nm.	Similar to MTT, MTS, and WST-1® assays, the formazan dye concentration is proportional to the intensity of the optical density and the cell viability.	130
Neutral red uptake assay	Neutral red uptake assay is based on the detection of neutral red (NR) dye inside the living cells. Viable cells can internalize the NR dye, which is taken up by the lysosome. This later is stained red. On the other hand, non-viable cells are not able to internalize this dye. After the lysosome staining,	Neutral red uptake assay provides a quantitative estimation of the number of viable cells. The cell viability is positively correlated to the amount of NR dye released and thus the optical density intensity.	131

	cells are washed, and the NR dye extracted. The optical density of NR dye is quantified at 540 nm.		
Alamar blue® assay	Alamar blue® (AB) is a water-soluble dye, which is not toxic to the cells. AB enters the cytosol, where it is reduced by mitochondrial enzymes in living cells. This reduction is accompanied by a change in the culture medium color from indigo blue to fluorescent pink. The change in color is easily measured by colorimetric or fluorometric reading.	The magnitude of AB reduction is correlated to the optical density intensity (or the fluorescence), which is proportional to the number of viable cells.	[127]
PicoGreen® assay	In the PicoGreen® fluorescence enhancement assay, the fluorochrome (PicoGreen) selectively binds double-stranded DNA (dsDNA) in living cells, leading to a fluorescence enhancement. The samples are excited at 480 nm, and their emission is set at 520-530 nm.	Fluorescence intensity amplitude is a consequence of a high amount of DNA in the living cell.	[132]
Annexin V-affinity assay	Annexin V staining assay allows sensitive and non-destructive analysis of apoptosis. Annexin V has a high affinity for phosphatidylserine. In healthy cells, phosphatidylserine is found in the inner leaflet of the lipid bilayer of the plasma membrane. During an apoptotic episode, the phosphatidylserine becomes exposed to the cell surface and is subsequently detected by the Annexin V labeled kit. Reading can be done either by flow cytometry or microscopy techniques.	In flow cytometry, living cells emit in the window of the fluorescent conjugate of Annexin V (e.g., dark green for Annexin V-FITC). In contrast, the apoptotic cells emit in a different window (e.g., blue).	[133]
Caspase 3 assay	The activation of caspase 3, a mammalian cysteine protease, plays a significant role in the apoptotic process. Caspase 3 is detected in the cell lysate by means of a fluorogenic substrate (N-acetyl-Asp-Glu-Val-Asp-7-amino-4-methylcoumarin). This substrate is cleaved by caspase 3, generating a fluorescent component (7-amino-4-methylcoumarin) that can be detected in a fluorescent reader ($\lambda_{ex} = 380$ nm) and $\lambda_{em} = 420$ nm).	Higher fluorescence emitted after caspase 3 assay corresponds to a high apoptotic process.	[134]
Cell membrane surface molecules assessment	In addition to the release of LDH and cytokines, it was reported that cells may over-express some molecules on their surface after contact with M&NPs. - CD11c: corresponds to an enhancement of macrophage maturation. - MHCII, CD1d: corresponds to an enhancement of antigen presentation. - CD40 and CD86: which translate a co-stimulation activity of the antigen-presenting cells. A way to access these molecules is by targeting them with specific staining after realizing an Fc-blocking.	The high fluorescence toward a targeted surface molecule compared to a negative control is interpreted by an over-expression of this surface molecule after the cell's contact with M&NPs.	[135]
RT-PCR	Reverse transcript polymerase chain reaction (RT-PCR) is based on the detection of bcl-2 and bax, which are specific gene primers associated with apoptosis. The calculation of the bax/bcl-2 ratio determines the susceptibility of a cell to undergo apoptosis. Accordingly, high values of this ratio are	When M&NPs are toxic to a cell, the apoptosis is translated by high values of bax/bcl-2 ratio.	[136]

	highly correlated with an apoptotic episode.		
CLSM	Confocal laser scanning microscopy is often used for analyzing the cell damage induced by the M&NPs. Appropriate staining of M&NPs and cells offers the possibility to visualize the internalization events and/or subcellular particle distribution. This technique was also used for visualizing cell shrinking and asymmetry during apoptosis.	CLSM allows the analysis of a cell apoptosis episode, the presence of white vesicles, and particle penetration inside the cell.	[137]
Electron microscopy techniques	Electron microscopy techniques are mainly used for the non-quantitative determination of cell apoptosis. They lead to the morphological characterization of dead cells and the determination of hallows regions in the dell membrane. Although very useful, these techniques are not often used as a first intention because, compared to other techniques, they are expensive, and they mainly allow a qualitative analysis.	Owing to their high resolution, electron microscopy techniques, when correctly set up, allow visualizing apoptotic events after cells treatment with M&NPs.	[138-140]

Table 3: Cytotoxicity of nonspherical M&NPs prepared from different materials.

M&NPs	Particle shape	Particle size (nm)	ζ (mV)	Incubation time	C (μg/mL)	Cell line	Cytotoxicity assay	Observation	Ref
Hydroxyapatite	Rod	96	-5.7	24 h	$10-300$	RAW 264.7[a] and BEAS-2B[b]	PicoGreen assay	PicoGreen assay revealed that the necrosis of BEAS-2B cells was tributary to the particle shape, which is in the order needles > plates > spheres > rods. Based on this assay, RAW264.7 was reported to be less sensitive to this test than BEAS-2B. Note that plate-shaped particles showed up to 15% reduction in dsDNA at 10 and 30 μg/mL. Overall, needles and plates were found to be more toxic according to this test.	141
	Plates	221×115	-9.7						
							ROS assay (DCFDA)	DCFDA assay (2',7'-dichlorodihydrofluorescein) is a fluorescent-dependent assay that allows the detection of ROS. The assay showed that, in BEAS-2B cells, regardless of the nanoparticle shape, ROS levels were at the same level as controls without nanoparticles. However, in RAW264.7 cells, needle-shaped particles generated increased ROS levels than the other shapes.	
	Spheres	92.3	-14.1						
	Needles	74.9	-4.8				Cytokine assay	Cytokine test revealed high expression of IL-6 in needle-shaped and plates particles. The IL-6 expression with the other nanoparticle shapes was comparable to the negative control. The same study did not reveal any difference in the TNF-α expression regardless of the particle shape.	
Silica	Long rods	278.1 (AR~4)	-30	24 h	$50-1000$	Caco2[c]	MTT assay	No significant changes in cell viability were reported with the cells after incubation with the nanoparticles, compared to control cells that were not exposed to nanoparticles. The authors explained the results by degrading the nanoparticles into nontoxic silicate ions,	111
	Short rods	289.0 (AR~2)							
	Spheres	250.9							

								regardless of their shape.	
Alumina	Rods	20 – 30 in width and 100 – 200 in length	N/A	72 h	15.6 – 8000	Astrocytes[d]	MTT assay	According to MTT results, nanorods exhibited higher toxicity for astrocytes than nanoflakes (LC_{50} value 3.6-fold higher for nanoflakes than that for nanorods).	142
							ROS assay	Both particles (nanorods and nanoflakes) induced ROS production. However, nanorods induced higher ROS generation than nanoflakes.	
	Flakes	20 – 30 in both width and length	N/A				Cytokine assay	The increase in the concentration of IL-1β, IL-2, and IL-6 was 1.5 to 2-fold higher after exposure of the cells to nanorods compared to nanoflakes.	
Silica	Worms	232 × 1348	87	72 h[1] 24 h[2]	0.0001 – 1000	RAW 264.7 and A549[e]	WST-8 assay, caspase 3, annexin V, and LDH assay	It was found that, at low concentrations (< 100 μg/mL), nanoparticle geometry played little to no role in mitochondrial function, membrane integrity, or cell death.	68
	Cylinders	214 × 428	79						
	Spheres	178	58						
Au	Rods	10 × 33	54.2	24 h	0 – 8000	SMMC 721[f], GES-1[g], and 4T1[h]	Cell counting kit (CCK-8) assay	CCK-8 assay revealed high cell viability (up to 80%) after the exposure with the nanoparticles, regardless of their shape at a high concentration of 3000 μg/mL. However, lower toxicity was noticed for spherical particles compared to rods and stars.	106
	Stars	15	-13.8						
	Spheres	15, 45 or 80	-8.8 to -25.4						
mPEG coated Au	Rods	~90.81	1.14	24 h	2.5 – 40	RAW 264.7[a]	CCK-8 assay	The three shapes of PEGylated Au nanoparticles were nontoxic for RAW 264.7 cells regardless of particle concentration.	105
	Stars	~82.88	-3.87						
	Triangles	~84.57	-1.88						

1/ incubation at 72 h for WST-1 assay. 2/ incubation at 24 h for LDH assay. a/ macrophage; Abelson murine leukaemia virus-transformed cell line. b/Primary and immortalized human bronchial epithelial cells. c/ Human colon tumor epithelial cells. d/ star-shaped glial cells in the brain and spinal cord. e/ human lung tumor epithelial cells. f/ human hepatocarcinoma cell line. g/ human gastric epithelial cell line. h/ mouse breast cancer cell line.

3. Theoretical approaches for particle endocytosis

3.1. Mechanical forces and energies over particle endocytosis

Forces and energies occurring during the interaction of a particle with a cell membrane are essential for cellular function and various biological processes. The creation of a vesicle wrapping the particle requires a mechanical force to deform the cell membrane and deviate from its spontaneous curvature denoted κ_0. Spontaneous curvature arises from combining several mechanisms, including membrane lipid composition and asymmetry, partitioning of transmembrane domains and protein crowding, insertion of hydrophobic protein motifs, the assembly of hydrophilic protein domains (e.g., clathrin, dynamin, caveolin), and macroscopic scaffolding by the cytoskeleton. For a review see, reference[143].

Contacting a particle with the cell membrane is an essential step for the beginning of the endocytic cascade, which results in particle wrapping, either through specific or non-specific mechanisms. When a particle docks on the cell membrane, various new tensions are created which, are drained by electrostatic forces, van der Waals forces, hydrophobic forces, and receptor-ligand interactions.[144] All these forces cumulate to form an adhesion strength (w) that creates the necessary imbalance to the resistance forces and thus starts the wrapping process.

Let us consider a simple example representing the interaction of a spherical particle with the cell membrane in Figure 4. Upon the interaction of a particle with the cell membrane surface, adhesion energy (ΔE) is generated at the particle-membrane interface. While unspecific ΔE is rapidly set up after particle interaction with the cell membrane, specific ΔE requires a longer time as it introduces a translational entropy. Once the particles are robustly attached to the cell membrane, the wrapping process begins, and the cell membrane deflects from its original curvature κ_0, relying primarily on a bending energy $C(\eta)$ and a stretching energy $\Gamma(\eta)$ (Figure 4). The wrapping extent (or the degree of wrapping) η (with $0 < \eta < 1$) is calculated from the ratio of the wrapped particle area to the total particle area. Additional deformation energy $\Lambda(\eta)$ stored in the curved membrane as represented in Figure 4.[145-147] Typically, for a fully wrapped particle, $\eta = 1$, the cell membrane comes back to its original curvature and $\Lambda = 0$. These two energies and the additional deformation energy are necessary for an effective wrapping of the particle (Figure 4). The total membrane deformation energy

(DE) required for an effective particle wrapping is the sum of $C(\eta)$, $\Gamma(\eta)$, and $\Lambda(\eta)$, as illustrated in Figure 4 and Eq.1.

$$DE = C(\eta) + \Gamma(\eta) + \Lambda(\eta) \qquad \text{Eq.1}$$

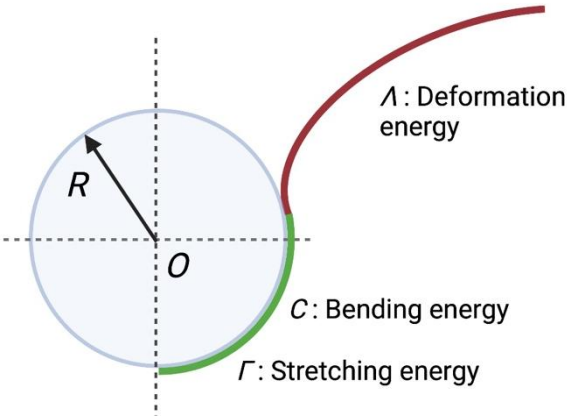

Figure 4: Schematic representation of membrane deformation energies over a wrapping episode. Adapted with permission from references[145-147]. R is the effective radius of the sphere.

Many theoretical studies were dedicated to understand how the cell membrane responds to external forces induced by the interaction of a particle.[32, 33, 145-152] Although various parameters are recurrently linked with a wrapping process; particle size undeniably plays a significant role. Based on energetic and kinetic considerations, it was possible to predict the minimum radius (R_{min}) upon which the endocytosis of a particle cannot be effective. If we consider a simple case in which a spherical particle interacts with a cell membrane through non-specific adhesion, the R_{min} is expressed by Eq.2.[147]

$$R_{min} = \sqrt{\frac{2B}{\alpha_{ns} - \sigma}} \qquad \text{Eq.2}$$

where B is the membrane bending modulus, α_{ns} represents the adhesion strength, and σ the membrane tension. For biological membranes, membrane bending modulus B, at a temperature of 300 K, is commonly expressed by Eq.3.[153]

$$B \sim 15 k_B T \qquad \text{Eq.3}$$

Thus, when α_{ns} is equal to $1\ k_B T/\text{nm}^2$, the minimum radius below which a wrapping process cannot occur is $R_{min} = 5$ nm.[147] In this situation, other endocytic pathways for cell entry, such as transmembrane diffusion, are privileged (Figure 1.4).

In the case of specific interactions between ligand-coated spherical or cylindrical particles with mobile receptors in the cell membrane, mathematical modeling revealed that particles

which size ranged from $10-100$ nm were endocytosed and exocytosed cells via wrapping events without implicating clathrin or caveolin coats.[154] According to the same authors, the optimal radius of spherical particles at which the endocytic time is the shortest was $27-30$ nm. Those predictions are in good agreement with several experimental data, revealing that the optimal radius for a maximum cell uptake was $\sim 25-30$ nm .[86, 155, 156] Thermodynamic models developed for specific interactions of ligand-coated nanoparticles and receptors in the cell membrane also predicted an optimal size for nanoparticle wrapping of $\sim 25-28$ nm.[150, 157] In the developed models, the ligands were assumed to be uniformly distributed on the particle surface with a density ξ_L and were immobile.[154, 157] The influence of ligand distribution on cellular uptake using coarse-grained molecular dynamins[158] or statistical dynamics model of endocytosis,[159] revealed that nanoparticles with homogenous ligand distribution are the most effectively wrapped.

Before the interaction, it was assumed that the receptors were uniformly distributed on the flat cell membrane with density ξ_0, and that their total number remains constant over wrapping (Figure 5). Upon the contact of the nanoparticle with the cell membrane, the mobile receptors diffused toward the contact area. The receptor density interacting with the ligands on the nanoparticle surface (ξ_b) became higher in the contact area. In contrast, a depletion zone with reduced receptor density (ξ_+) is formed in the noninteracting region of the cell membrane (Figure 5). ξ_b reaches a maximum value when each ligand interacts with one receptor ($\xi_b = \xi_L$). In the model developed by Gao et al.,[154] the nanoparticle was considered either cylindrical or spherical. Notably, if we assume that the cell size was much larger than nanoparticle size, the initial state of the cell membrane was presented as flat. Simulation results revealed that an optimal receptor density ratio ($\bar{\xi} = \xi_0/\xi_L$) is required for effective wrapping. As the $\bar{\xi}$ increased, the optimal wrapping radius and optimal wrapping time decreased. In contrast, for small $\bar{\xi}$, the optimal particle radius and wrapping time increased.[154]

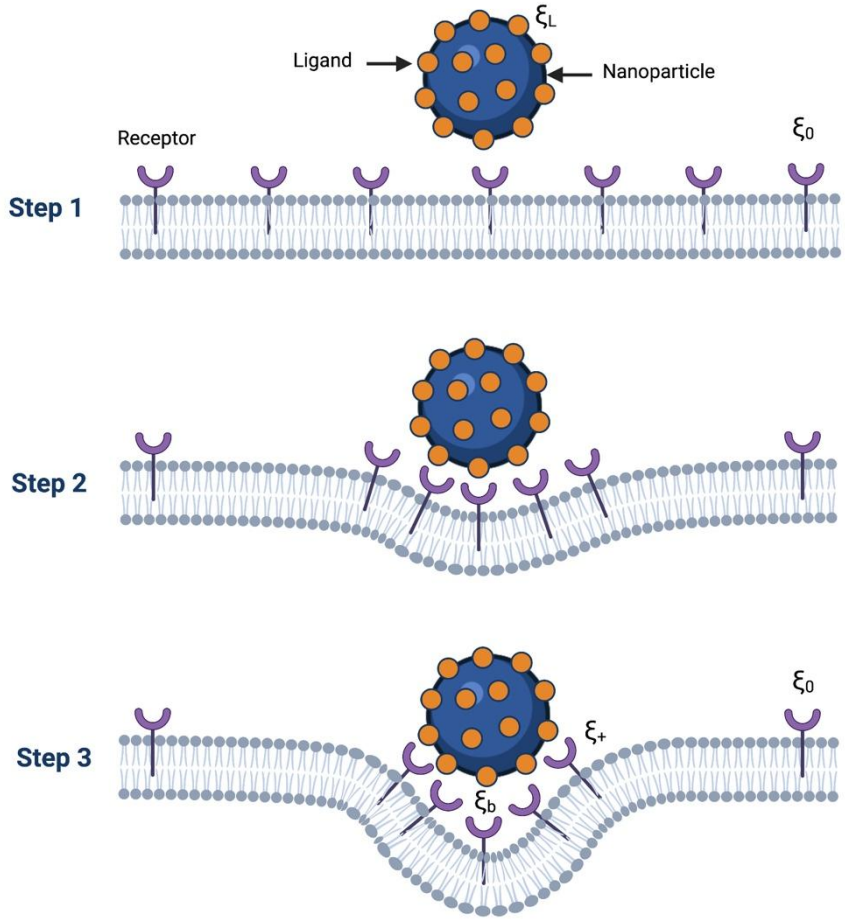

Figure 5: Schematic representation of the different steps for receptor-mediated wrapping of a spherical nanoparticle. Step 1: Nonwrapped state. Step 2: binding state. Step 3: partially wrapped state. ξ_0 is the receptor density in the remote region. ξ_+ is the receptor density in the depletion region. ξ_b is the density of the receptor in the binding region. ξ_L is the ligand density on the nanoparticle surface.

3.2. Shape effect

While the fundamental biophysical behaviors of cell membrane deformation over a wrapping episode remain applicable for nonspherical particles, they exhibited some differences in the wrapping mechanism compared with spherical ones. Understanding the energetics of a nonspherical particle is more complicated due to the various orientations possible upon the interaction with the cell membrane. Thanks to computational modeling at different length scales, the energetics for nonspherical particle wrapping were better understood. Typically, coarse-grained models and numerical calculations of membrane mechanics based on energy minimization revealed that the endocytosis mechanism of a nonspherical particle is defined as a sequence of four different steps:[31-34] a nonwrapped state, a binding state, a partially wrapped state, and a complete wrapped state, where the particle is completely engulfed by the cell membrane (Figure 6). A partially wrapped state could be further subdivided into two other steps: the shallow wrapped state, which comes right after an

effective particle binding to the surface area, and a deep-wrapped state mainly characterized by a deeper nanoparticle penetration and a higher surface tension of the cell (Figure 6).

Interestingly, several groups agree that nonspherical particles can enter the cell through different modes (Figure 6):[31, 34, 160-162] a submarine mode (or parallel adhering mode), when the particle is presented to the cell membrane via its long axis and a rocket mode (or perpendicular entry mode) when the long axis is perpendicular to the cell membrane. Another case is also possible. It consists of the competition between both submarine and rocket modes, characterized by the rotation of the particle over a wrapping episode (Figure 6.a and 6.b).[34, 163]

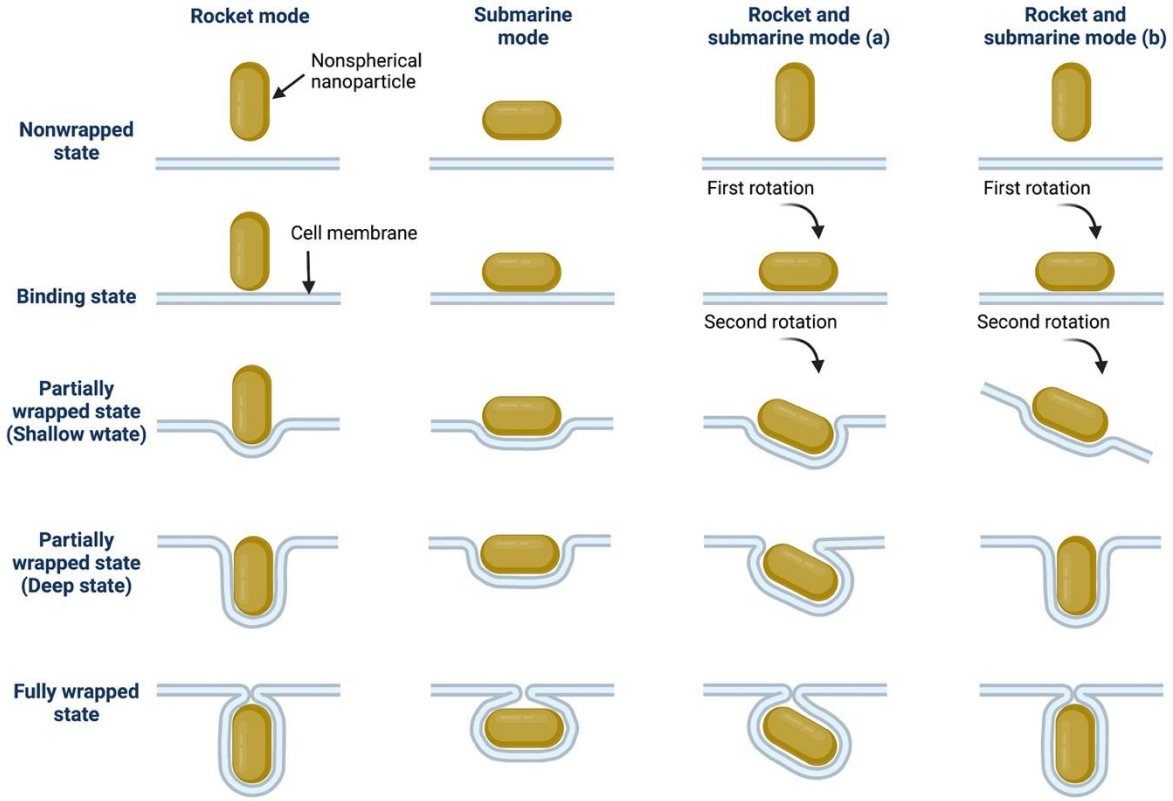

Figure 6: Illustration of the different entry modes of nonspherical nanoparticles according to numerical simulations.

Within the same framework, modeling of particle membrane interaction revealed that the wrapping of cube-like and rod-like particles compared to the wrapping of spheres and ellipsoids is different.[31] Complete wrapping of cube-like particles required increased adhesion energy in the lateral edges to back up the deformation energy of the lower edge and increased deformation energy of the upper edge.[31] For cube-like particles, the adhesion strength to reach a deep wrapping state is ~2 times higher than for a sphere with an equal surface area. This was accompanied by increased membrane tension and adhesion strength. For a complete wrapping of Hauser's cube, the adhesion strength was found to be ~3 times higher than for a

sphere. Moreover, very high adhesion strength is necessary for the complete wrapping of cube-like particles. On the other hand, particle shape dictated its internalization mode. For example, a nanorod with AR ~ 1.5 switched from a rocket position to a submarine position, but for sharper edges, rocket mode predominates.[31]

In another embodiment, molecular dynamic simulations on a coarse-grained model revealed that the local curvature radius and the sharpness of the edges of the nanoparticle in contact with the membrane played a significant role in the wrapping process.[161] Indeed, the passive endocytosis process of ligand-coated rod particles was thermodynamically favorable, while cylinders did not undergo complete wrapping, but they remained attached to the membrane. Notably, in this article, rod particles were referred to as spherocylinders (cylinders with hemispherical caps at both ends). The cylinders had a diameter D, while the whole rod's length was L. The AR was ~ 1 or ~ 2, as calculated from the ratio L/D. The results showed that, upon the interaction with the membrane, the rods changed their orientation from perpendicular to parallel (Figure 6.a). The same investigation revealed that the endocytosis of rods was more thermodynamically favorable than spheres.[161]

However, opposite results were found with PEG-coated nanoparticles with variable shapes and using large-scale dissipative particle dynamics simulations.[164] The simulations revealed that, at low PEG density, spherical nanoparticles had the fastest internalization rate, followed by cubes, then rods and disks.[164] The molecular simulations showed that the entry pathway of nanoparticles with high AR (rods and disks) was highly dependent on the contact angle with the membrane. When the nanoparticles with high AR interacted with a cell membrane through their major axis, the large membrane deformation and time-consuming particle orientation delayed the internalization. The same study showed that star-shaped nanoparticles exhibited fast wrapping by the cell membrane, which is similar to spherical nanoparticles. It was noticed that when the nanoparticles were fully covered with PEG, the effective shapes of all the particles were close to spherical. In these conditions, the shape of the nanoparticle core is invisible to the cell membrane (see Figure 9 in reference[164]).

4. Shape-dependent behaviors in the systemic circulation

Protein corona represents the first barrier a particle encounters when administrated in the blood because thousands of different blood proteins will competitively bind to the particle surface.[165, 166] This phenomenon complicates any prediction of cell interactions, biodistribution, and toxicity because it is the protein corona/M&NP complex, rather than the

bare M&NPs interacting with biological machinery.[167] Furthermore, targeting properties of M&NPs are hindered by protein adsorption on functional ligands, preventing their interaction with the corresponding cell receptors.[49] After adsorption of opsonins on the M&NP surface and phagocytosis, the particles will be directed to MPS organs, such as the liver and spleen. Indeed, $30-99\%$ of administered M&NPs accumulate and sequester in the liver.[168] To reduce non-specific adsorption of proteins on the M&NPs surface, a plethora of research works were focused on grafting hydrophilic polymers such as PEG on the particle surface.[169] This strategy reduced opsonization leading to the escape of immediate sequestration by the immune system after administration in the blood. Unfortunately, now, there is a piece of evidence that repeated administration of PEG-coated nanoparticles in the blood induces hypersensitivity reactions described as complement activation-related pseudoallergy (CARPA).[170] Several strategies have been envisioned so far to reduce the adsorption of opsonins on the particle surface. Unlike size and surface properties (e.g., hydrophilic/hydrophobic ratio, steric hindrance), the effect of M&NP shape on opsonization was understudied. Some data were reported on the impact of the radius of curvature of M&NPs in the composition and conformation of adsorbed proteins by using spherical particles with variable sizes. For example, previous works on spherical gold nanoparticles showed that big particle size, and consequently high radius of curvature, affects protein corona structure as proteins may stretch to fit the large particle surface. Smaller dimensions of isotropic nanoparticles resulted in decreased interaction with proteins, causing fewer structural changes.[171-174] For anisotropic nanoparticles with high AR, one expects large proteins aligning along the long axis to fit on the nanoparticle surface.[175, 176] Large proteins, on the other hand, may not fit in small spaces and hence be excluded from the small dimension of the nanoparticles. Additionally, anisotropic particle geometry does affect complement activation. The IgM and the classical and lectin pathway convertase (C4b2a) have cross-sectional diameters of ~ 40 nm and ~ 30 nm, respectively, making its assembly and deposition onto the surface of nanoparticles with high curvature rather tricky.[177-179] Therefore, particle dimensions lower than 30 nm, and depending on their surface chemistry, may not efficiently trigger calcium-sensitive pathways of complement activation, while a surface-bound C3b is expected to occupy an area of 40 nm.[180]

Specific interactions of nonspherical M&NPs with blood proteins, with macrophages and polymorphonuclear neutrophils, as well as the dynamic behaviors of the particles under shear flow, significantly impact their biodistribution (Table 4). The most reported tendency is that

nonspherical M&NPs had a prolonged circulation time in the blood,[2, 41, 62, 181, 182] and had a preferential accumulation in specific organs,[2, 17, 39, 181, 183-187] compared to spherical particles. For example, rod-shaped PEGylated Au particles (10×45 nm) had a longer circulation time in the blood than spherical particles (50 nm in diameter), which preferentially accumulated in the liver.[182] Exceptional long circulation times (up to 1 week) were reported with highly flexible filamentous micelles ($\sim 20 - 60$ nm in cross-sectional diameter and a tuneable length $\sim 2 - 18$ μm) after intravenous injection in rats.[2] Comparatively, PEGylated spherical vesicles (120 nm) with similar surface properties to filomicelles were cleared within 48 h. Several mechanisms are involved in the prolonged circulation time of filamentous micelles. One possible explanation could be their low phagocytosis profiles. Indeed, high AR and high flexibility of the filamentous micelles reduced their interaction with macrophages, required for their internalization. Previous research on spherical nanoparticles with variable rigidity showed that rigid particles displayed higher uptake by macrophages than soft ones.[30, 188] Rapid elimination of stiff nanoparticles was correlated to their higher macrophage capture.[30] When filomicelle rigidity was increased by crosslinking, they were cleared within a few hours.

On the other hand, the same study revealed that filomicelle size is a critical attribute for their interaction with macrophages and subsequent internalization.[2] Long worms were less captured by macrophages than short filomicelles or spheres, thus reducing their clearance. Similarly, by tuning the shape of polystyrene or Au particles from spheres to rods or elliptical disks, macrophage uptake was reduced, circulation $t_{1/2}$ in mice blood was increased, while liver uptake was decreased.[62, 182]

Contrarily to spheres, the disks, targeted to intracellular adhesion molecule (ICAM-1), preferentially accumulated in the lungs. The lung to liver accumulation was 1.7-fold higher for anti-ICAM-coated polystyrene rods (125×500 nm) than for spherical particles (200 nm diameter).[189] Shape-specific tissue accumulation was also observed for anti-transferrin-conjugated rod particles for brain targeting. Transferrin-coated rods exhibited ~ 7 fold higher accumulation in the brain compared with transferrin-coated spherical particles.[189] In vitro experiments performed on a synthetic microvascular network model showed that rod particles exhibited higher binding to the walls under shear flow than spherical particles. This phenomenon, known as margination, was tackled a decade ago for nonspherical M&NPs.[190-192] In a theoretical study, Toy et al.,[190] concluded that Au nanorods had an 8-fold higher margination rate than nanospheres. Another investigation revealed that both size and

morphology had a consequent impact on the margination and adhesion of M&NPs.[193] Their experimental analysis, conducted on spherical, oblate, prolate, and rod M&NPs, revealed a higher margination and adhesion of micro-scale nonspherical particles than nano-scale spherical counterparts. Additionally, Da Silva-Candal et al.,[194] found that rod particles have a more targeting efficiency to the endothelium receptors than spherical particles. Spherical particles are more likely to follow the shear forces' direction and continue their way in the streamline. Once they marginate, nonspherical particles display another characteristic which is their ability to set up a multi-point contact with the receptors in the vessel wall due to their bigger surface area and lower number of curvatures. Several experimental and theoretical studies confirmed the ability of elongated M&NPs to marginate to the vascular wall of the vessel and subsequent extravasation under shear and pressure forces.[195] For review articles, see references[196, 197].

The tendency of rod-like or disk-like particles to align the blood flow and to extravasate partly explains higher accumulation in tumoral tissues (Table 4).[182, 184, 187, 198-200] The biodistribution of porous silicon discoidal particles (400 × 600 nm and 400 × 1000 nm, height × diameter) in a murine bearing cancer model was found to be up to 5 times higher than with spherical particles (600 nm diameter).[200] Spherical particles accumulated more prominently in the liver. Rod-like particles (80 × 320 nm) loaded with docetaxel showed reduced phagocytosis by macrophages and prolonged circulation time in the blood compared to spherical particles, resulting from higher tumor exposure to the drug.[181] Additionally, nonspherical M&NPs showed improved diffusion through tumoral tissues compared with spheroidal particles.[201] Chauhan et al.,[199] revealed that nanorods (15 × 54 nm) diffused in a tumor-mimetic collagen gel ~5 times faster than the nanospheres (35 nm). The same nanorods penetrated tumors ~4 times faster than nanospheres in mice bearing orthotopic tumors.[199] The two particles had similar plasma $t_{1/2}$ and clearance in mice.

To sum up this section, although it is not possible to make a clear conclusion on the in vivo fate of nonspherical M&NPs particles compared to spherical ones, there is a piece of evidence that particles with a high AR and high flexibility had prolonged circulation in the blood. The increased accumulation of elongated particles in tumoral tissues is promising. It could lead to an increase in the efficacy of chemotherapeutics and a reduction of the side effects by limiting the accumulation in healthy tissues. Those findings should trigger further studies to design more effective nanomedicines by acting on M&NP shape.

Table 4: Comparison of the effect of M&NP morphology on their behavior *in vivo* regarding their biodistribution, clearance, and therapeutic efficiency.

M&NPs	Route of administration (Animal used)	Shape and size	Studied property	Observations	Ref
Mesoporous silica nanoparticles	Intravenous (mice)	Long rods (720 nm in length, AR ~5) Short rods (185 nm in length, AR ~1.5)	Biodistribution (2 h, 24 h, and 7 days after injection)	- Two hours after injection, both short and long PEGylated nanorods accumulated mainly in the liver, spleen, and lung (over 80% of the injected dose). Short PEGylated nanorods were more easily trapped in the liver, while long PEGylated nanorods accumulated preferentially in the lung. However, 24 h after injection, both short and long PEGylated nanorods were trapped in the spleen > lung > liver.	202
			Excretion	- Short PEGylated nanorods had a faster clearance than long PEGylated nanorods in urine and feces.	
			Biocompatibility	- There is no association between the shape and the toxicity of the nanoparticles.	
Micelles	Intravenous (mice and rats)	Filomicelles ($\sim 20-60$ nm) × ($2-18$ μm)	Biodistribution (ap to 6 days)	- The blood circulation of filomicelles was up to 6 days, while spherical vesicles of similar chemistry were cleared within two days after injection to rats. - Four days after injection, the filomicelles accumulated in the liver > spleen > kidney > lung.	2
			Treatment	- 7 days after injection to tumor-bearing mice, paclitaxel-loaded filomicelles can more effectively reduce tumor size compared to free paclitaxel	
Micelles	Intravenous (tumor-bearing mice)	Filomicelles Spheres	Biodistribution (after 24 h)	- Filomicelles remained in the blood for at least 24 h. - 24 h after injection, uptake was higher in the MPS organs (liver > spleen > lungs > heart > tumor > kidney > brain).	203
			Treatment	- The high accumulation of paclitaxel-loaded filomicelles produced a higher mass shrinkage and tumor cell death regarding the spherical control.	
Rod-shaped	Intravenous	Short rods (~18 ×	Biodistribution	- The results are represented as total tissue penetration	204

nucleoprotein nanoparticles derived from tobacco mosaic virus (Either PEGylated or RGD targeted)	(tumor-bearing mice)	60 nm, AR ~3.5) Medium rods (~18 × 130 nm, AR ~7) Long rods (~18 × 300 nm, AR ~16)		(bladder + liver + spleen). PEGylated short rods showed a peak tissue accumulation at 2 h, while PEGylated long rods showed a peak tissue accumulation at 6 h.	
			Clearance	- PEGylated long rods were cleared by the RE system as the nanoparticles were cleared via the liver and spleen. - PEGylated short rods were mainly cleared via the bladder suggesting a renal filtration elimination.	
			Accumulation in the tumors	- The accumulation of both stealth and targeted nanorods in the tumors was AR-dependent. PEGylated short rods showed the highest accumulation in tumors, followed by median and long nanorods. RGD-targeted median nanorods showed the best accumulation in tumors.	
PEGylated tobacco mosaic virus-derived nanoparticles	Intravenous	Rods (~18 × 130 nm, AR ~7) Spheres (54 nm measured by TEM)	Biodistribution	- Rods and spherical particles accumulated mainly in the liver and spleen.	[205]
			Clearance	- Spherical particles showed shorter circulation in the blood and were more rapidly eliminated than rods. They were no longer detected after 24 h of injection. - Rod particles were detectable in the liver and spleen after 24 h.	
Liposomes	Intravenous (rats)	Spheres Disks	Biodistribution	- The discoidal shape enhanced by nearly 2 folds the circulation half-life of liposomes in a rat model.	[1]
Polymeric nanoparticles (polymerization induced self-assembly)	Intravenous (tumor-bearing mice)	Rods (37 nm in diameter and 350 − 500 nm in length) Worms (44.5 nm in diameter and 1 − 2 μm in length) Spheres (~21 nm or 33 nm)	Biodistribution	- Worms displayed the highest accumulation in the spleen > liver > lungs > kidneys.	[206]
			Clearance	- Regardless of their morphology, the particles were cleared from the blood circulation 2 days post-delivery.	
			Accumulation in the tumors	- The highest tumor accumulation was obtained with small and spherical micelles, whereas the lowest tumor accumulation was observed for the worms.	

5. Summary and future directions

While a consensus on the M&NPs shape dependence on biological processes was reached, some contradictory results should be pointed out at several levels. The major issue is related to a discrepancy in particle composition, size, shape, surface properties. In several investigations, the surface area and volume of M&NPs with different shapes are not always kept constant and the biological process may be rather driven by other particle parameters than geometry. The isolation of the parameters one by one should lead to a better understanding of the exact role of the shape on biological processes. Such understanding requires robust technological tools for designing particles with controlled properties in a reproducible manner. Not only by handling the shape but also 3D dimensions, surface properties, and particle mechanical behaviors, because those parameters are interconnected. The development of novel technological tools for designing nonspherical M&NPs with a simultaneous control of their properties is still needed. Indeed, each technique used for preparing nonspherical particles has its advantages and drawbacks. For example, mainly micrometer sized particles with different shapes and AR can be obtained by photolithography[207] and microfluidics.[208] By self-assembly of small amphiphilic molecules, a variety of morphologies are harvested, including rods, nanoribbons, filomicelles, and worms.[209] Generally speaking, shape modification is mediated by the composition of the amphiphilic molecules. Ring-opened benzyl-L-glutamate led to particles with different AR (up to 3.5).[210] However, particles with different AR do not have comparable surface properties since the shape is controlled by polymer molecular weight. In some cases, nonspherical M&NPs did not always show a shape stability. For example, elliptical particles switch their shape to a sphere.[211] The particles were obtained by physical deformation of poly(lactide-*co*-glycolide) spheres contained in a film composed of poly(vinyl alcohol). In a recent investigation, Ahmed et al.,[23] succeeded in preparing shape-stable elliptical particles by film stretching technique. However, the same study highlighted some difficulties in removing poly(vinyl alcohol) from the particle preparation.[23] In addition to surface modification following the adsorption of poly(vinyl alcohol), moving from spherical to elongated shape could also modify the particle mechanical properties, leading to mixed parameters. The exact implication of each parameter in the biological process could be complicated.

Modeling the interaction of M&NPs with the cell membrane offers the opportunity to isolate the parameters conferring a better understanding of fundamental events over particle

wrapping. Such knowledge will pave the way toward the correct interpretation of the experimental data of the endocytosis process in different applications, including pathogen infections and drug delivery. Furthermore, the models developed for particle wrapping could be applicable to a wide range of biological processes such as viral entry to cells, intracellular trafficking, and exocytosis. The basic structures representing only the double bilayer membrane and receptors could be further improved by adding complex structures of the cell membrane. The effect of clathrin and other envelope proteins should also be considered. Finally, it is necessary to consider physiologically relevant conditions such as osmotic pressure.

On the other hand, in several reports, it was found that the biological effect was correlated to the purification level of the preparations. For carbon nanotubes, cytotoxicity was rather due to metal traces contaminants than the carbon nanotube itself.[212] For Au particles, the cytotoxicity was mainly due to extrachemicals present in the preparation. The free detergent hexadecyltrimethylammonium bromide, due to incomplete purification of the Au nanorods, was shown to be toxic to the cell membrane.[112, 213, 214] Standardization of the properties of the preparations, their purification, and the conditions for cytotoxicity experiments is necessary to investigate the effect of particle shape accurately.

Furthermore, the experimental conditions for the biological evaluations, such as the cell lines, the ratio between the cells and the M&NPs, and the animal model used, are of crucial importance. For example, it was shown that the same preparation was more rapidly eliminated from the mice blood than rats. Comparisons between M&NPs can be reasonably drawn between experiments conducted on similar cells and animals.

Another challenge in the future is related to the lack of standardization of the physicochemical techniques for the characterization of M&NPs dimensions. In several studies, the particle size was given for spherical and nonspherical particles, while nonspherical particles are typically characterized by at least two dimensions (e.g., length, width, thickness). Furthermore, most of the investigations used dynamic light scattering techniques to characterize the size of nonspherical particles. However, this technique, based on the Stocks-Einstein equation, was not adapted to compare the size of particles with different diffusion coefficients. Indeed, in a recent investigation, Diaz-Salmeron et al.,[10] revealed that, in static conditions, hyaluronan particles with a high AR, designated nanoplatelets, exhibited more linear trajectories and faster diffusion in water than nanospheres. Electron microscopy techniques could provide information on the particle shape

and dimensions. However, imaging techniques that require the drying of the sample (e.g., TEM, SEM, and AFM imaging in the air), did not lead to a correct determination of the exact particle dimensions in liquid conditions, and in turn, it could lead to a misinterpretation of the results obtained in culture media or in vivo. A better analysis of M&NPs dimensions was provided by cryo-TEM, cryo-SEM, and AFM in liquid conditions. It was observed that the height cross-section of flat particles obtained by hierarchical self-assembly of α-cyclodextrin and hydrophobically modified hyaluronan in liquid were ~4.5-fold lower than that measured in dry conditions.[11] An accurate characterization thus is essential for understanding and the correct interpretation of the biological behaviors.

In short, despite the interest in particle shape in biological processes, the issues mentioned above should be addressed to speed-up the translation of nonspherical particles into the clinic. Indeed, despite the efforts in developing shape-controlled M&NPs, only a few examples are commercially available. Besides inorganic particles, PRINT™ particles that are uniform in shape and bioresorbable (LIQ001) were tested in the clinic to improve immune response and efficacy of seasonal influenza vaccine. The therapeutic and commercial success of disk-like liposomes (Amphotec®) and Ribbon-like particles (Abelcet®) should pave the way to additional investigations for other applications.

6. Funding

Author K.B. received funding from the Institut Universitaire de France and the ANR-17-CE09-0038-1.

7. References

1. Li, S.; Nickels, J.; Palmer, A. F., Liposome-encapsulated actin–hemoglobin (LEAcHb) artificial blood substitutes. *Biomaterials* **2005,** *26* (17), 3759-3769.
2. Geng, Y.; Dalhaimer, P.; Cai, S.; Tsai, R.; Tewari, M.; Minko, T.; Discher, D. E., Shape effects of filaments versus spherical particles in flow and drug delivery. *Nature Nanotechnology* **2007,** *2* (4), 249.
3. d'Agosto, F.; Rieger, J.; Lansalot, M., RAFT-Mediated Polymerization-Induced Self-Assembly. *Angewandte Chemie International Edition* **2020,** *59* (22), 8368-8392.
4. Rieger, J., Guidelines for the synthesis of block copolymer particles of various morphologies by RAFT dispersion polymerization. *Macromolecular rapid communications* **2015,** *36* (16), 1458-1471.
5. Mellot, G. l. Combinaison de la chimie supramoléculaire et de la PISA contrôlée par RAFT pour synthétiser des nanofibres dans l'eau. Sorbonne université, 2019.
6. Han, S.; Pensec, S.; Yilmaz, D.; Lorthioir, C.; Jestin, J.; Guigner, J.-M.; Niepceron, F.; Rieger, J.; Stoffelbach, F.; Nicol, E.; Colombani, O.; Bouteiller, L., Straightforward preparation of supramolecular Janus nanorods by hydrogen bonding of end-functionalized polymers. *Nature Communications* **2020,** *11* (1), 1-6.

7. Galus, A.; Mallet, J.-M.; Lembo, D.; Cagno, V.; Djabourov, M.; Lortat-Jacob, H.; Bouchemal, K., Hexagonal-shaped chondroitin sulfate self-assemblies have exalted anti-HSV-2 activity. *Carbohydrate Polymers* **2016,** *136*, 113-120.
8. Carn, F.; Nowak, S.; Chaab, I.; Diaz-Salmeron, R.; Djabourov, M.; Bouchemal, K., Autoassemblies of α-cyclodextrin and grafted polysaccharides: Crystal structure and specific properties of the platelets. *The Journal of Physical Chemistry B* **2018,** *122* (22), 6055-6063.
9. Diaz-Salmeron, R.; Chaab, I.; Carn, F.; Djabourov, M.; Bouchemal, K., Pickering emulsions with α-cyclodextrin inclusions: Structure and thermal stability. *Journal of Colloid and Interface Science* **2016,** *482*, 48-57.
10. Diaz-Salmeron, R.; Da Costa, A.; Michel, J.-P.; Ponchel, G.; Bouchemal, K., Real-Time Visualization of Morphology-Dependent Self-Motion of Hyaluronic Acid Nanomaterials in Water. *International Journal of Pharmaceutics* **2021**, 121172.
11. Diaz-Salmeron, R.; Michel, J.-P.; Hadji, H.; Gout, E.; Vivès, R. R.; Ponchel, G.; Bouchemal, K., Role of the interactions with CD44 and supported bilayer membranes in the cellular uptake of soft multivalent hyaluronan nanoparticles. *Colloids and Surfaces B: Biointerfaces* **2021**, 111916.
12. Diaz-Salmeron, R.; Ponchel, G.; Bouchemal, K., Hierarchically built hyaluronan nano-platelets have symmetrical hexagonal shape, flattened surfaces and controlled size. *European Journal of Pharmaceutical Sciences* **2019,** *133*, 251-263.
13. Diaz-Salmeron, R.; Ponchel, G.; Gallard, J.-F.; Bouchemal, K., Hierarchical supramolecular platelets from hydrophobically-modified polysaccharides and α-cyclodextrin: Effect of hydrophobization and α-cyclodextrin concentration on platelet formation. *International Journal of Pharmaceutics* **2018,** *548* (1), 227-236.
14. Lembo, D.; Donalisio, M.; Laine, C.; Cagno, V.; Civra, A.; Bianchini, E. P.; Zeghbib, N.; Bouchemal, K., Auto-associative heparin nanoassemblies: a biomimetic platform against the heparan sulfate-dependent viruses HSV-1, HSV-2, HPV-16 and RSV. *European Journal of Pharmaceutics and Biopharmaceutics* **2014,** *88* (1), 275-282.
15. Enlow, E. M.; Luft, J. C.; Napier, M. E.; DeSimone, J. M., Potent engineered PLGA nanoparticles by virtue of exceptionally high chemotherapeutic loadings. *Nano letters* **2011,** *11* (2), 808-813.
16. Gratton, S. E.; Napier, M. E.; Ropp, P. A.; Tian, S.; DeSimone, J. M., Microfabricated particles for engineered drug therapies: elucidation into the mechanisms of cellular internalization of PRINT particles. *Pharmaceutical Research* **2008,** *25* (12), 2845-2852.
17. Gratton, S. E.; Pohlhaus, P. D.; Lee, J.; Guo, J.; Cho, M. J.; DeSimone, J. M., Nanofabricated particles for engineered drug therapies: A preliminary biodistribution study of PRINT™ nanoparticles. *Journal of Controlled Release* **2007,** *121* (1-2), 10-18.
18. Gratton, S. E.; Ropp, P. A.; Pohlhaus, P. D.; Luft, J. C.; Madden, V. J.; Napier, M. E.; DeSimone, J. M., The effect of particle design on cellular internalization pathways. *Proceedings of the National Academy of Sciences* **2008,** *105* (33), 11613-11618.
19. Florez, L.; Herrmann, C.; Cramer, J. M.; Hauser, C. P.; Koynov, K.; Landfester, K.; Crespy, D.; Mailänder, V., How shape influences uptake: interactions of anisotropic polymer nanoparticles and human mesenchymal stem cells. *Small* **2012,** *8* (14), 2222-2230.
20. Champion, J. A.; Katare, Y. K.; Mitragotri, S., Making polymeric micro-and nanoparticles of complex shapes. *Proceedings of the National Academy of Sciences* **2007,** *104* (29), 11901-11904.
21. Champion, J. A.; Mitragotri, S., Role of target geometry in phagocytosis. *Proceedings of the National Academy of Sciences* **2006,** *103* (13), 4930-4934.
22. Palazzo, C.; Ponchel, G.; Vachon, J. J.; Villebrun, S.; Agnely, F.; Vauthier, C., Obtaining nonspherical poly (alkylcyanoacrylate) nanoparticles by the stretching method applied with a marketed water-soluble film. *International Journal of Polymeric Materials and Polymeric Biomaterials* **2017,** *66* (8), 416-424.
23. Ahmed, Z.; Ponchel, G.; Bouchemal, K., Shape stability of ellipsoidal nanomaterials prepared by physical deformation. *International Journal of Pharmaceutics* **2021,** *609*, 121178.

24. Fakhri, N.; MacKintosh, F. C.; Lounis, B.; Cognet, L.; Pasquali, M., Brownian motion of stiff filaments in a crowded environment. *Science* **2010,** *330* (6012), 1804-1807.
25. Han, Y.; Alsayed, A. M.; Nobili, M.; Zhang, J.; Lubensky, T. C.; Yodh, A. G., Brownian motion of an ellipsoid. *Science* **2006,** *314* (5799), 626-630.
26. Anselmo, A. C.; Modery-Pawlowski, C. L.; Menegatti, S.; Kumar, S.; Vogus, D. R.; Tian, L. L.; Chen, M.; Squires, T. M.; Sen Gupta, A.; Mitragotri, S., Platelet-like nanoparticles: mimicking shape, flexibility, and surface biology of platelets to target vascular injuries. *ACS nano* **2014,** *8* (11), 11243-11253.
27. Vahidkhah, K.; Bagchi, P., Microparticle shape effects on margination, near-wall dynamics and adhesion in a three-dimensional simulation of red blood cell suspension. *Soft Matter* **2015,** *11* (11), 2097-2109.
28. Gentile, F.; Chiappini, C.; Fine, D.; Bhavane, R.; Peluccio, M.; Cheng, M. M.-C.; Liu, X.; Ferrari, M.; Decuzzi, P., The effect of shape on the margination dynamics of non-neutrally buoyant particles in two-dimensional shear flows. *Journal of biomechanics* **2008,** *41* (10), 2312-2318.
29. Gentile, F.; Curcio, A.; Indolfi, C.; Ferrari, M.; Decuzzi, P., The margination propensity of spherical particles for vascular targeting in the microcirculation. *Journal of nanobiotechnology* **2008,** *6* (1), 9.
30. Anselmo, A. C.; Zhang, M.; Kumar, S.; Vogus, D. R.; Menegatti, S.; Helgeson, M. E.; Mitragotri, S., Elasticity of nanoparticles influences their blood circulation, phagocytosis, endocytosis, and targeting. *ACS nano* **2015,** *9* (3), 3169-3177.
31. Dasgupta, S.; Auth, T.; Gompper, G., Shape and orientation matter for the cellular uptake of nonspherical particles. *Nano Letters* **2014,** *14* (2), 687-693.
32. Bahrami, A. H.; Lipowsky, R.; Weikl, T. R., The role of membrane curvature for the wrapping of nanoparticles. *Soft Matter* **2016,** *12* (2), 581-587.
33. Van Der Wel, C.; Vahid, A.; Šarić, A.; Idema, T.; Heinrich, D.; Kraft, D. J., Lipid membrane-mediated attraction between curvature inducing objects. *Scientific reports* **2016,** *6* (1), 1-10.
34. Huang, C.; Zhang, Y.; Yuan, H.; Gao, H.; Zhang, S., Role of nanoparticle geometry in endocytosis: laying down to stand up. *Nano letters* **2013,** *13* (9), 4546-4550.
35. Doshi, N.; Mitragotri, S., Macrophages recognize size and shape of their targets. *PloS one* **2010,** *5* (4), e10051.
36. Sharma, G.; Valenta, D. T.; Altman, Y.; Harvey, S.; Xie, H.; Mitragotri, S.; Smith, J. W., Polymer particle shape independently influences binding and internalization by macrophages. *Journal of Controlled Release* **2010,** *147* (3), 408-412.
37. Zhang, Y.; Nayak, T. R.; Hong, H.; Cai, W., Graphene: a versatile nanoplatform for biomedical applications. *Nanoscale* **2012,** *4* (13), 3833-3842.
38. Zhang, Y.; Tekobo, S.; Tu, Y.; Zhou, Q.; Jin, X.; Dergunov, S. A.; Pinkhassik, E.; Yan, B., Permission to enter cell by shape: nanodisk vs nanosphere. *ACS Applied Materials & Interfaces* **2012,** *4* (8), 4099-4105.
39. Agarwal, R.; Singh, V.; Jurney, P.; Shi, L.; Sreenivasan, S.; Roy, K., Mammalian cells preferentially internalize hydrogel nanodiscs over nanorods and use shape-specific uptake mechanisms. *Proceedings of the National Academy of Sciences* **2013,** *110* (43), 17247-17252.
40. He, Y.; Park, K., Effects of the microparticle shape on cellular uptake. *Molecular pharmaceutics* **2016,** *13* (7), 2164-2171.
41. Hu, X.; Hu, J.; Tian, J.; Ge, Z.; Zhang, G.; Luo, K.; Liu, S., Polyprodrug amphiphiles: hierarchical assemblies for shape-regulated cellular internalization, trafficking, and drug delivery. *Journal of the American Chemical Society* **2013,** *135* (46), 17617-17629.
42. Chu, Z.; Zhang, S.; Zhang, B.; Zhang, C.; Fang, C.-Y.; Rehor, I.; Cigler, P.; Chang, H.-C.; Lin, G.; Liu, R., Unambiguous observation of shape effects on cellular fate of nanoparticles. *Scientific Reports* **2014,** *4*, 4495.
43. Chu, Z.; Miu, K.; Lung, P.; Zhang, S.; Zhao, S.; Chang, H.-C.; Lin, G.; Li, Q., Rapid endosomal escape of prickly nanodiamonds: implications for gene delivery. *Scientific reports* **2015,** *5* (1), 1-8.

44. Chaturbedy, P.; Kumar, M.; Salikolimi, K.; Das, S.; Sinha, S. H.; Chatterjee, S.; Suma, B.; Kundu, T. K.; Eswaramoorthy, M., Shape-directed compartmentalized delivery of a nanoparticle-conjugated small-molecule activator of an epigenetic enzyme in the brain. *Journal of Controlled Release* **2015,** *217*, 151-159.
45. Xu, Z. P.; Niebert, M.; Porazik, K.; Walker, T. L.; Cooper, H. M.; Middelberg, A. P.; Gray, P. P.; Bartlett, P. F.; Lu, G. Q. M., Subcellular compartment targeting of layered double hydroxide nanoparticles. *Journal of Controlled Release* **2008,** *130* (1), 86-94.
46. Walkey, C. D.; Chan, W. C., Understanding and controlling the interaction of nanomaterials with proteins in a physiological environment. *Chemical Society Reviews* **2012,** *41* (7), 2780-2799.
47. Nel, A. E.; Mädler, L.; Velegol, D.; Xia, T.; Hoek, E. M.; Somasundaran, P.; Klaessig, F.; Castranova, V.; Thompson, M., Understanding biophysicochemical interactions at the nano–bio interface. *Nature Materials* **2009,** *8* (7), 543.
48. Corbo, C.; Molinaro, R.; Parodi, A.; Toledano Furman, N. E.; Salvatore, F.; Tasciotti, E., The impact of nanoparticle protein corona on cytotoxicity, immunotoxicity and target drug delivery. *Nanomedicine* **2016,** *11* (1), 81-100.
49. Salvati, A.; Pitek, A. S.; Monopoli, M. P.; Prapainop, K.; Bombelli, F. B.; Hristov, D. R.; Kelly, P. M.; Åberg, C.; Mahon, E.; Dawson, K. A., Transferrin-functionalized nanoparticles lose their targeting capabilities when a biomolecule corona adsorbs on the surface. *Nature Nanotechnology* **2013,** *8* (2), 137-143.
50. Barbero, F.; Russo, L.; Vitali, M.; Piella, J.; Salvo, I.; Borrajo, M. L.; Busquets-Fité, M.; Grandori, R.; Bastús, N. G.; Casals, E. In *Formation of the protein corona: the interface between nanoparticles and the immune system*, Seminars in Immunology, Elsevier: 2017; pp 52-60.
51. Flaherty, D., *Immunology for Pharmacy-E-Book*. Elsevier Health Sciences: 2014.
52. Fais, S., Cannibalism: a way to feed on metastatic tumors. *Cancer letters* **2007,** *258* (2), 155-164.
53. Brill-Karniely, Y.; Dror, D.; Duanis-Assaf, T.; Goldstein, Y.; Schwob, O.; Millo, T.; Orehov, N.; Stern, T.; Jaber, M.; Loyfer, N., Triangular correlation (TrC) between cancer aggressiveness, cell uptake capability, and cell deformability. *Science advances* **2020,** *6* (3), eaax2861.
54. Kaksonen, M.; Roux, A., Mechanisms of clathrin-mediated endocytosis. *Nature reviews Molecular cell biology* **2018,** *19* (5), 313-326.
55. Bareford, L. M.; Swaan, P. W., Endocytic mechanisms for targeted drug delivery. *Advanced drug delivery reviews* **2007,** *59* (8), 748-758.
56. Liu, Z.; Roche, P. A., Macropinocytosis in phagocytes: regulation of MHC class-II-restricted antigen presentation in dendritic cells. *Frontiers in physiology* **2015,** *6*, 1.
57. Haigler, H. T.; McKANNA, J. A.; Cohen, S., Rapid stimulation of pinocytosis in human carcinoma cells A-431 by epidermal growth factor. *The Journal of cell biology* **1979,** *83* (1), 82-90.
58. Swanson, J. A., Shaping cups into phagosomes and macropinosomes. *Nature reviews Molecular cell biology* **2008,** *9* (8), 639-649.
59. Buckley, C. M.; King, J. S., Drinking problems: mechanisms of macropinosome formation and maturation. *The FEBS journal* **2017,** *284* (22), 3778-3790.
60. Rossman, J. S.; Leser, G. P.; Lamb, R. A., Filamentous influenza virus enters cells via macropinocytosis. *Journal of virology* **2012,** *86* (20), 10950-10960.
61. Caì, Y.; Postnikova, E. N.; Bernbaum, J. G.; Yú, S.; Mazur, S.; Deiuliis, N. M.; Radoshitzky, S. R.; Lackemeyer, M. G.; McCluskey, A.; Robinson, P. J., Simian hemorrhagic fever virus cell entry is dependent on CD163 and uses a clathrin-mediated endocytosis-like pathway. *Journal of virology* **2015,** *89* (1), 844-856.
62. Muro, S.; Garnacho, C.; Champion, J. A.; Leferovich, J.; Gajewski, C.; Schuchman, E. H.; Mitragotri, S.; Muzykantov, V. R., Control of endothelial targeting and intracellular delivery of therapeutic enzymes by modulating the size and shape of ICAM-1-targeted carriers. *Molecular Therapy* **2008,** *16* (8), 1450-1458.

63. Yoo, J. W.; Doshi, N.; Mitragotri, S., Endocytosis and intracellular distribution of PLGA particles in endothelial cells: effect of particle geometry. *Macromolecular Rapid Communications* **2010,** *31* (2), 142-148.
64. Decuzzi, P.; Ferrari, M., The receptor-mediated endocytosis of nonspherical particles. *Biophysical Journal* **2008,** *94* (10), 3790-3797.
65. Zhao, X.; Lu, D.; Hao, F.; Liu, R., Exploring the diameter and surface dependent conformational changes in carbon nanotube-protein corona and the related cytotoxicity. *Journal of Hazardous Materials* **2015,** *292*, 98-107.
66. Huang, X.; Teng, X.; Chen, D.; Tang, F.; He, J., The effect of the shape of mesoporous silica nanoparticles on cellular uptake and cell function. *Biomaterials* **2010,** *31* (3), 438-448.
67. Meng, H.; Yang, S.; Li, Z.; Xia, T.; Chen, J.; Ji, Z.; Zhang, H.; Wang, X.; Lin, S.; Huang, C., Aspect ratio determines the quantity of mesoporous silica nanoparticle uptake by a small GTPase-dependent macropinocytosis mechanism. *ACS Nano* **2011,** *5* (6), 4434-4447.
68. Herd, H. L.; Malugin, A.; Ghandehari, H., Silica nanoconstruct cellular toleration threshold in vitro. *Journal of Controlled Release* **2011,** *153* (1), 40-48.
69. Yoon, K. W., Dead cell phagocytosis and innate immune checkpoint. *BMB reports* **2017,** *50* (10), 496.
70. Gustafson, H. H.; Holt-Casper, D.; Grainger, D. W.; Ghandehari, H., Nanoparticle uptake: the phagocyte problem. *Nano today* **2015,** *10* (4), 487-510.
71. Vonarbourg, A.; Passirani, C.; Saulnier, P.; Benoit, J.-P., Parameters influencing the stealthiness of colloidal drug delivery systems. *Biomaterials* **2006,** *27* (24), 4356-4373.
72. Bodman-Smith, K. B.; Melendez, A. J.; Campbell, I.; Harrison, P. T.; Allen, J. M.; Raynes, J. G., C-reactive protein-mediated phagocytosis and phospholipase D signalling through the high-affinity receptor for immunoglobulin G (FcγRI). *Immunology* **2002,** *107* (2), 252-260.
73. Gordon, S., Macrophage Activation in: Encyclopaedia of Immunology 2nd ed., DJ Weatherall, JGG Ledingham, and DA Warrell eds. Academic Press, London: 1998.
74. Vachon, E.; Martin, R.; Kwok, V.; Cherepanov, V.; Chow, C.-W.; Doerschuk, C. M.; Plumb, J.; Grinstein, S.; Downey, G. P., CD44-mediated phagocytosis induces inside-out activation of complement receptor-3 in murine macrophages. *Blood, The Journal of the American Society of Hematology* **2007,** *110* (13), 4492-4502.
75. Hiemstra, P. S.; Daha, M. R., Opsonization. **1998**.
76. May, R. C.; Machesky, L. M., Phagocytosis and the actin cytoskeleton. *Journal of cell science* **2001,** *114* (6), 1061-1077.
77. Jaumouillé, V.; Grinstein, S., Molecular mechanisms of phagosome formation. *Myeloid Cells in Health and Disease: A Synthesis* **2017**, 507-526.
78. Kaufmann, S. H.; Collins, H. L.; Schaible, U. E., Immune responses to intracellular bacteria. In *Clinical immunology: principles and practice*, Mosby: 2008; pp 389-409.
79. Wong, C.-O.; Gregory, S.; Hu, H.; Chao, Y.; Sepúlveda, V. E.; He, Y.; Li-Kroeger, D.; Goldman, W. E.; Bellen, H. J.; Venkatachalam, K., Lysosomal degradation is required for sustained phagocytosis of bacteria by macrophages. *Cell host & microbe* **2017,** *21* (6), 719-730. e6.
80. Paul, D.; Achouri, S.; Yoon, Y.-Z.; Herre, J.; Bryant, C. E.; Cicuta, P., Phagocytosis dynamics depends on target shape. *Biophysical journal* **2013,** *105* (5), 1143-1150.
81. Aderem, A., How to eat something bigger than your head. *Cell* **2002,** *110* (1), 5-8.
82. Champion, J. A.; Mitragotri, S., Shape induced inhibition of phagocytosis of polymer particles. *Pharmaceutical research* **2009,** *26* (1), 244-249.
83. Rolland, J. P.; Maynor, B. W.; Euliss, L. E.; Exner, A. E.; Denison, G. M.; DeSimone, J. M., Direct fabrication and harvesting of monodisperse, shape-specific nanobiomaterials. *Journal of the American Chemical Society* **2005,** *127* (28), 10096-10100.
84. Kelly, J. Y.; DeSimone, J. M., Shape-specific, monodisperse nano-molding of protein particles. *Journal of the American Chemical Society* **2008,** *130* (16), 5438-5439.
85. Alemdaroglu, F. E.; Alemdaroglu, N. C.; Langguth, P.; Herrmann, A., DNA block copolymer micelles–a combinatorial tool for cancer nanotechnology. *Advanced Materials* **2008,** *20* (5), 899-902.

86. Chithrani, B. D.; Ghazani, A. A.; Chan, W. C., Determining the size and shape dependence of gold nanoparticle uptake into mammalian cells. *Nano Letters* **2006,** *6* (4), 662-668.
87. Yanes, R. E.; Tarn, D.; Hwang, A. A.; Ferris, D. P.; Sherman, S. P.; Thomas, C. R.; Lu, J.; Pyle, A. D.; Zink, J. I.; Tamanoi, F., Involvement of lysosomal exocytosis in the excretion of mesoporous silica nanoparticles and enhancement of the drug delivery effect by exocytosis inhibition. *Small* **2013,** *9* (5), 697-704.
88. Kim, D.; Gao, Z. G.; Lee, E. S.; Bae, Y. H., In vivo evaluation of doxorubicin-loaded polymeric micelles targeting folate receptors and early endosomal pH in drug-resistant ovarian cancer. *Molecular pharmaceutics* **2009,** *6* (5), 1353-1362.
89. Fernández, M.; Javaid, F.; Chudasama, V., Advances in targeting the folate receptor in the treatment/imaging of cancers. *Chemical science* **2018,** *9* (4), 790-810.
90. Marshall, K. E.; Vadukul, D. M.; Staras, K.; Serpell, L. C., Misfolded amyloid-β-42 impairs the endosomal–lysosomal pathway. *Cellular and molecular life sciences* **2020,** *77* (23), 5031-5043.
91. Moku, G.; Gulla, S. K.; Nimmu, N. V.; Khalid, S.; Chaudhuri, A., Delivering anti-cancer drugs with endosomal pH-sensitive anti-cancer liposomes. *Biomaterials science* **2016,** *4* (4), 627-638.
92. Xu, E.; Saltzman, W. M.; Piotrowski-Daspit, A. S., Escaping the endosome: Assessing cellular trafficking mechanisms of non-viral vehicles. *Journal of Controlled Release* **2021**.
93. Chaudhary, N.; Weissman, D.; Whitehead, K. A., mRNA vaccines for infectious diseases: principles, delivery and clinical translation. *Nature Reviews Drug Discovery* **2021**, 1-22.
94. Hajj, K. A.; Whitehead, K. A., Tools for translation: non-viral materials for therapeutic mRNA delivery. *Nature Reviews Materials* **2017,** *2* (10), 1-17.
95. Pantarotto, D.; Briand, J.-P.; Prato, M.; Bianco, A., Translocation of bioactive peptides across cell membranes by carbon nanotubes. *Chemical Communications* **2004,** (1), 16-17.
96. Kam, N. W. S.; Liu, Z.; Dai, H., Carbon nanotubes as intracellular transporters for proteins and DNA: an investigation of the uptake mechanism and pathway. *Angewandte Chemie International Edition* **2006,** *45* (4), 577-581.
97. Jin, H.; Heller, D. A.; Strano, M. S., Single-particle tracking of endocytosis and exocytosis of single-walled carbon nanotubes in NIH-3T3 cells. *Nano letters* **2008,** *8* (6), 1577-1585.
98. Desai, P.; Venkataramanan, A.; Schneider, R.; Jaiswal, M. K.; Carrow, J. K.; Purwada, A.; Singh, A.; Gaharwar, A. K., Self-assembled, ellipsoidal polymeric nanoparticles for intracellular delivery of therapeutics. *Journal of Biomedical Materials Research Part A* **2018,** *106* (7), 2048-2058.
99. Yang, H.; Chen, Z.; Zhang, L.; Yung, W. Y.; Leung, K. C. F.; Chan, H. Y. E.; Choi, C. H. J., Mechanism for the cellular uptake of targeted gold nanorods of defined aspect ratios. *Small* **2016,** *12* (37), 5178-5189.
100. Shimoni, O.; Yan, Y.; Wang, Y.; Caruso, F., Shape-dependent cellular processing of polyelectrolyte capsules. *ACS nano* **2013,** *7* (1), 522-530.
101. Shi, J.; Choi, J. L.; Chou, B.; Johnson, R. N.; Schellinger, J. G.; Pun, S. H., Effect of polyplex morphology on cellular uptake, intracellular trafficking, and transgene expression. *ACS nano* **2013,** *7* (12), 10612-10620.
102. Huang, L. H.; Han, J.; Ouyang, J. M.; Gui, B. S., Shape-dependent adhesion and endocytosis of hydroxyapatite nanoparticles on A7R5 aortic smooth muscle cells. *Journal of cellular physiology* **2020,** *235* (1), 465-479.
103. Li, Z.; Sun, L.; Zhang, Y.; Dove, A. P.; O'Reilly, R. K.; Chen, G., Shape effect of glyco-nanoparticles on macrophage cellular uptake and immune response. *ACS macro letters* **2016,** *5* (9), 1059-1064.
104. Herd, H.; Daum, N.; Jones, A. T.; Huwer, H.; Ghandehari, H.; Lehr, C.-M., Nanoparticle geometry and surface orientation influence mode of cellular uptake. *ACS nano* **2013,** *7* (3), 1961-1973.
105. Xie, X.; Liao, J.; Shao, X.; Li, Q.; Lin, Y., The effect of shape on cellular uptake of gold nanoparticles in the forms of stars, rods, and triangles. *Scientific reports* **2017,** *7* (1), 1-9.

106. Ding, L.; Yao, C.; Yin, X.; Li, C.; Huang, Y.; Wu, M.; Wang, B.; Guo, X.; Wang, Y.; Wu, M., Size, shape, and protein corona determine cellular uptake and removal mechanisms of gold nanoparticles. *Small* **2018,** *14* (42), 1801451.
107. Scarpa, E.; De Pace, C.; Joseph, A. S.; de Souza, S. C.; Poma, A.; Liatsi-Douvitsa, E.; Contini, C.; De Matteis, V.; Martí, J. S.; Battaglia, G., Tuning cell behavior with nanoparticle shape. *PloS one* **2020,** *15* (11), e0240197.
108. Pantarotto, D.; Singh, R.; McCarthy, D.; Erhardt, M.; Briand, J. P.; Prato, M.; Kostarelos, K.; Bianco, A., Functionalized carbon nanotubes for plasmid DNA gene delivery. *Angewandte Chemie International Edition* **2004,** *43* (39), 5242-5246.
109. Hasan, W.; Chu, K.; Gullapalli, A.; Dunn, S. S.; Enlow, E. M.; Luft, J. C.; Tian, S.; Napier, M. E.; Pohlhaus, P. D.; Rolland, J. P., Delivery of multiple siRNAs using lipid-coated PLGA nanoparticles for treatment of prostate cancer. *Nano letters* **2012,** *12* (1), 287-292.
110. Morgan, E.; Wupperfeld, D.; Morales, D.; Reich, N., Shape matters: Gold nanoparticle shape impacts the biological activity of siRNA delivery. *Bioconjugate chemistry* **2019,** *30* (3), 853-860.
111. Zhao, Y.; Wang, Y.; Ran, F.; Cui, Y.; Liu, C.; Zhao, Q.; Gao, Y.; Wang, D.; Wang, S., A comparison between sphere and rod nanoparticles regarding their in vivo biological behavior and pharmacokinetics. *Scientific reports* **2017,** *7* (1), 1-11.
112. Fernando, D.; Sulthana, S.; Vasquez, Y., Cellular uptake and cytotoxicity of varying aspect ratios of gold nanorods in HeLa cells. *ACS Applied Bio Materials* **2020,** *3* (3), 1374-1384.
113. Ji, Z.; Wang, X.; Zhang, H.; Lin, S.; Meng, H.; Sun, B.; George, S.; Xia, T.; Nel, A. E.; Zink, J. I., Designed synthesis of CeO2 nanorods and nanowires for studying toxicological effects of high aspect ratio nanomaterials. *ACS nano* **2012,** *6* (6), 5366-5380.
114. Tschopp, J.; Schroder, K., NLRP3 inflammasome activation: The convergence of multiple signalling pathways on ROS production? *Nature reviews immunology* **2010,** *10* (3), 210-215.
115. Wang, X.; Xia, T.; Addo Ntim, S.; Ji, Z.; Lin, S.; Meng, H.; Chung, C.-H.; George, S.; Zhang, H.; Wang, M., Dispersal state of multiwalled carbon nanotubes elicits profibrogenic cellular responses that correlate with fibrogenesis biomarkers and fibrosis in the murine lung. *ACS nano* **2011,** *5* (12), 9772-9787.
116. Sweeney, S.; Grandolfo, D.; Ruenraroengsak, P.; Tetley, T. D., Functional consequences for primary human alveolar macrophages following treatment with long, but not short, multiwalled carbon nanotubes. *International journal of nanomedicine* **2015,** *10*, 3115.
117. Sweeney, S.; Berhanu, D.; Misra, S. K.; Thorley, A. J.; Valsami-Jones, E.; Tetley, T. D., Multi-walled carbon nanotube length as a critical determinant of bioreactivity with primary human pulmonary alveolar cells. *Carbon* **2014,** *78*, 26-37.
118. Oberdörster, G.; Stone, V.; Donaldson, K., Toxicology of nanoparticles: a historical perspective. *Nanotoxicology* **2007,** *1* (1), 2-25.
119. Poland, C. A.; Duffin, R.; Kinloch, I.; Maynard, A.; Wallace, W. A.; Seaton, A.; Stone, V.; Brown, S.; MacNee, W.; Donaldson, K., Carbon nanotubes introduced into the abdominal cavity of mice show asbestos-like pathogenicity in a pilot study. *Nature nanotechnology* **2008,** *3* (7), 423-428.
120. Kang, S.; Kim, J.-E.; Kim, D.; Woo, C. G.; Pikhitsa, P. V.; Cho, M.-H.; Choi, M., Comparison of cellular toxicity between multi-walled carbon nanotubes and onion-like shell-shaped carbon nanoparticles. *Journal of Nanoparticle Research* **2015,** *17* (9), 1-11.
121. Nahle, S.; Safar, R.; Grandemange, S.; Foliguet, B.; Lovera-Leroux, M.; Doumandji, Z.; Le Faou, A.; Joubert, O.; Rihn, B.; Ferrari, L., Single wall and multiwall carbon nanotubes induce different toxicological responses in rat alveolar macrophages. *Journal of Applied Toxicology* **2019,** *39* (5), 764-772.
122. Almutary, A.; Sanderson, B., The MTT and crystal violet assays: potential confounders in nanoparticle toxicity testing. *International journal of toxicology* **2016,** *35* (4), 454-462.
123. Kroll, A.; Pillukat, M. H.; Hahn, D.; Schnekenburger, J., Interference of engineered nanoparticles with in vitro toxicity assays. *Archives of toxicology* **2012,** *86* (7), 1123-1136.
124. Braydich-Stolle, L.; Hussain, S.; Schlager, J. J.; Hofmann, M.-C., In vitro cytotoxicity of nanoparticles in mammalian germline stem cells. *Toxicological sciences* **2005,** *88* (2), 412-419.

125. Rösslein, M.; Elliott, J. T.; Salit, M.; Petersen, E. J.; Hirsch, C.; Krug, H. F.; Wick, P., Use of cause-and-effect analysis to design a high-quality nanocytotoxicology assay. *Chemical research in toxicology* **2015,** *28* (1), 21-30.
126. Kumar, P.; Nagarajan, A.; Uchil, P. D., Analysis of cell viability by the lactate dehydrogenase assay. *Cold Spring Harbor Protocols* **2018,** *2018* (6), pdb. prot095497.
127. Tzankova, V.; Aluani, D.; Yordanov, Y.; Valoti, M.; Frosini, M.; Spassova, I.; Kovacheva, D.; Tzankov, B., In vitro toxicity evaluation of lomefloxacin-loaded MCM-41 mesoporous silica nanoparticles. *Drug and chemical toxicology* **2021,** *44* (3), 238-249.
128. Zhang, Y.; Dai, M.; Yuan, Z., Methods for the detection of reactive oxygen species. *Analytical Methods* **2018,** *10* (38), 4625-4638.
129. Bakan, B.; Gülcemal, S.; Akgöl, S.; Hoet, P. H.; Yavaşoğlu, N. Ü. K., Synthesis, characterization and toxicity assessment of a new polymeric nanoparticle, l-glutamic acid-gp (HEMA). *Chemico-biological interactions* **2020,** *315*, 108870.
130. Lutter, A.-H.; Scholka, J.; Richter, H.; Anderer, U., Applying XTT, WST-1, and WST-8 to human chondrocytes: A comparison of membrane-impermeable tetrazolium salts in 2D and 3D cultures. *Clinical hemorheology and microcirculation* **2017,** *67* (3-4), 327-342.
131. Hu, W.; Culloty, S.; Darmody, G.; Lynch, S.; Davenport, J.; Ramirez-Garcia, S.; Dawson, K.; Lynch, I.; Doyle, H.; Sheehan, D., Neutral red retention time assay in determination of toxicity of nanoparticles. *Marine environmental research* **2015,** *111*, 158-161.
132. Heng, B. C.; Das, G. K.; Zhao, X.; Ma, L.-L.; Tan, T. T.-Y.; Ng, K. W.; Loo, J. S.-C., Comparative cytotoxicity evaluation of lanthanide nanomaterials on mouse and human cell lines with metabolic and DNA-quantification assays. *Biointerphases* **2010,** *5* (3), FA88-FA97.
133. Demchenko, A. P., Beyond annexin V: fluorescence response of cellular membranes to apoptosis. *Cytotechnology* **2013,** *65* (2), 157-172.
134. Fujita, N.; Nagahashi, A.; Nagashima, K.; Rokudai, S.; Tsuruo, T., Acceleration of apoptotic cell death after the cleavage of Bcl-X L protein by caspase-3-like proteases. *Oncogene* **1998,** *17* (10), 1295-1304.
135. Palomäki, J.; Karisola, P.; Pylkkänen, L.; Savolainen, K.; Alenius, H., Engineered nanomaterials cause cytotoxicity and activation on mouse antigen presenting cells. *Toxicology* **2010,** *267* (1-3), 125-131.
136. Wang, X.; Xia, Y.; Liu, L.; Liu, M.; Gu, N.; Guang, H.; Zhang, F., Comparison of MTT assay, flow cytometry, and RT-PCR in the evaluation of cytotoxicity of five prosthodontic materials. *Journal of Biomedical Materials Research Part B: Applied Biomaterials* **2010,** *95* (2), 357-364.
137. Dekaliuk, M.; Pyrshev, K.; Demchenko, A., Visualization and detection of live and apoptotic cells with fluorescent carbon nanoparticles. *Journal of nanobiotechnology* **2015,** *13* (1), 1-8.
138. Taatjes, D. J.; Sobel, B. E.; Budd, R. C., Morphological and cytochemical determination of cell death by apoptosis. *Histochemistry and cell biology* **2008,** *129* (1), 33-43.
139. Malli, S.; Bories, C.; Bourge, M.; Loiseau, P. M.; Bouchemal, K., Surface-dependent endocytosis of poly(isobutylcyanoacrylate) nanoparticles by *Trichomonas vaginalis*. *International Journal of Pharmaceutics* **2018,** *548* (1), 276-287.
140. Malli, S.; Pomel, S.; Ayadi, Y.; Delomenie, C.; Da Costa, A.; Loiseau, P. M.; Bouchemal, K., Topically applied chitosan-coated poly(isobutylcyanoacrylate) nanoparticles are active against cutaneous Leishmaniasis by accelerating lesion healing and reducing the parasitic load. *ACS Applied Bio Materials* **2019,** *2* (6), 2573-2586.
141. Zhao, X.; Ng, S.; Heng, B. C.; Guo, J.; Ma, L.; Tan, T. T. Y.; Ng, K. W.; Loo, S. C. J., Cytotoxicity of hydroxyapatite nanoparticles is shape and cell dependent. *Archives of toxicology* **2013,** *87* (6), 1037-1052.
142. Dong, L.; Tang, S.; Deng, F.; Gong, Y.; Zhao, K.; Zhou, J.; Liang, D.; Fang, J.; Hecker, M.; Giesy, J. P., Shape-dependent toxicity of alumina nanoparticles in rat astrocytes. *Science of the Total Environment* **2019,** *690*, 158-166.
143. McMahon, H. T.; Boucrot, E., Membrane curvature at a glance. *Journal of cell science* **2015,** *128* (6), 1065-1070.

144. Villanueva-Flores, F.; Castro-Lugo, A.; Ramírez, O. T.; Palomares, L. A., Understanding cellular interactions with nanomaterials: towards a rational design of medical nanodevices. *Nanotechnology* **2020,** *31* (13), 132002.
145. Deserno, M.; Bickel, T., Wrapping of a spherical colloid by a fluid membrane. *EPL (Europhysics Letters)* **2003,** *62* (5), 767.
146. Deserno, M., Elastic deformation of a fluid membrane upon colloid binding. *Physical Review E* **2004,** *69* (3), 031903.
147. Zhang, S.; Gao, H.; Bao, G., Physical principles of nanoparticle cellular endocytosis. *ACS nano* **2015,** *9* (9), 8655-8671.
148. De, R., A general model of focal adhesion orientation dynamics in response to static and cyclic stretch. *Communications biology* **2018,** *1* (1), 1-7.
149. Brill-Karniely, Y., Mechanical Measurements of Cells Using AFM: 3D or 2D Physics? *Frontiers in Bioengineering and Biotechnology* **2020,** *8*.
150. Zhang, S.; Li, J.; Lykotrafitis, G.; Bao, G.; Suresh, S., Size-dependent endocytosis of nanoparticles. *Advanced materials* **2009,** *21* (4), 419-424.
151. Bao, G.; Bao, X. R., Shedding light on the dynamics of endocytosis and viral budding. *Proceedings of the National Academy of Sciences* **2005,** *102* (29), 9997-9998.
152. Rangamani, P.; Mandadap, K. K.; Oster, G., Protein-induced membrane curvature alters local membrane tension. *Biophysical journal* **2014,** *107* (3), 751-762.
153. Bell, G. I., Models for the specific adhesion of cells to cells. *Science* **1978,** *200* (4342), 618-627.
154. Gao, H.; Shi, W.; Freund, L. B., Mechanics of receptor-mediated endocytosis. *Proceedings of the National Academy of Sciences* **2005,** *102* (27), 9469-9474.
155. Osaki, F.; Kanamori, T.; Sando, S.; Sera, T.; Aoyama, Y., A quantum dot conjugated sugar ball and its cellular uptake. On the size effects of endocytosis in the subviral region. *Journal of the American Chemical Society* **2004,** *126* (21), 6520-6521.
156. Chithrani, B. D.; Chan, W. C., Elucidating the mechanism of cellular uptake and removal of protein-coated gold nanoparticles of different sizes and shapes. *Nano Letters* **2007,** *7* (6), 1542-1550.
157. Yuan, H.; Zhang, S., Effects of particle size and ligand density on the kinetics of receptor-mediated endocytosis of nanoparticles. *Applied Physics Letters* **2010,** *96* (3), 033704.
158. Schubertová, V.; Martinez-Veracoechea, F. J.; Vácha, R., Influence of ligand distribution on uptake efficiency. *Soft Matter* **2015,** *11* (14), 2726-2730.
159. Li, L.; Zhang, Y.; Wang, J., Effects of ligand distribution on receptor-diffusion-mediated cellular uptake of nanoparticles. *Royal Society open science* **2017,** *4* (5), 170063.
160. Yi, X.; Shi, X.; Gao, H., A universal law for cell uptake of one-dimensional nanomaterials. *Nano letters* **2014,** *14* (2), 1049-1055.
161. Vácha, R.; Martinez-Veracoechea, F. J.; Frenkel, D., Receptor-mediated endocytosis of nanoparticles of various shapes. *Nano letters* **2011,** *11* (12), 5391-5395.
162. Chen, L.; Xiao, S.; Zhu, H.; Wang, L.; Liang, H., Shape-dependent internalization kinetics of nanoparticles by membranes. *Soft Matter* **2016,** *12* (9), 2632-2641.
163. Chen, L.; Li, X.; Zhang, Y.; Chen, T.; Xiao, S.; Liang, H., Morphological and mechanical determinants of cellular uptake of deformable nanoparticles. *Nanoscale* **2018,** *10* (25), 11969-11979.
164. Li, Y.; Kröger, M.; Liu, W. K., Shape effect in cellular uptake of PEGylated nanoparticles: comparison between sphere, rod, cube and disk. *Nanoscale* **2015,** *7* (40), 16631-16646.
165. Cedervall, T.; Lynch, I.; Lindman, S.; Berggård, T.; Thulin, E.; Nilsson, H.; Dawson, K. A.; Linse, S., Understanding the nanoparticle–protein corona using methods to quantify exchange rates and affinities of proteins for nanoparticles. *Proceedings of the National Academy of Sciences* **2007,** *104* (7), 2050-2055.
166. Barrán-Berdón, A. L.; Pozzi, D.; Caracciolo, G.; Capriotti, A. L.; Caruso, G.; Cavaliere, C.; Riccioli, A.; Palchetti, S.; Laganà, A., Time evolution of nanoparticle–protein corona in human plasma: relevance for targeted drug delivery. *Langmuir* **2013,** *29* (21), 6485-6494.

167. Walczyk, D.; Bombelli, F. B.; Monopoli, M. P.; Lynch, I.; Dawson, K. A., What the cell "sees" in bionanoscience. *Journal of the American Chemical Society* **2010,** *132* (16), 5761-5768.
168. Zhang, Y.-N.; Poon, W.; Tavares, A. J.; McGilvray, I. D.; Chan, W. C., Nanoparticle–liver interactions: cellular uptake and hepatobiliary elimination. *Journal of controlled release* **2016,** *240*, 332-348.
169. Gref, R.; Minamitake, Y.; Peracchia, M. T.; Trubetskoy, V.; Torchilin, V.; Langer, R., Biodegradable long-circulating polymeric nanospheres. *Science* **1994,** *263* (5153), 1600-1603.
170. Kozma, G. T.; Mészáros, T.; Vashegyi, I.; Fülöp, T. s.; Örfi, E.; Dézsi, L.; Rosivall, L.; Bavli, Y.; Urbanics, R.; Mollnes, T. E., Pseudo-anaphylaxis to polyethylene glycol (PEG)-coated liposomes: Roles of Anti-PEG IgM and complement activation in a porcine model of human infusion reactions. *ACS Nano* **2019,** *13* (8), 9315-9324.
171. Tenzer, S.; Docter, D.; Rosfa, S.; Wlodarski, A.; Kuharev, J. r.; Rekik, A.; Knauer, S. K.; Bantz, C.; Nawroth, T.; Bier, C., Nanoparticle size is a critical physicochemical determinant of the human blood plasma corona: a comprehensive quantitative proteomic analysis. *ACS Nano* **2011,** *5* (9), 7155-7167.
172. Lundqvist, M.; Stigler, J.; Elia, G.; Lynch, I.; Cedervall, T.; Dawson, K. A., Nanoparticle size and surface properties determine the protein corona with possible implications for biological impacts. *Proceedings of the National Academy of Sciences* **2008,** *105* (38), 14265-14270.
173. Dobrovolskaia, M. A.; Patri, A. K.; Zheng, J.; Clogston, J. D.; Ayub, N.; Aggarwal, P.; Neun, B. W.; Hall, J. B.; McNeil, S. E., Interaction of colloidal gold nanoparticles with human blood: effects on particle size and analysis of plasma protein binding profiles. *Nanomedicine: Nanotechnology, Biology and Medicine* **2009,** *5* (2), 106-117.
174. Koegler, P.; Clayton, A.; Thissen, H.; Santos, G. N. C.; Kingshott, P., The influence of nanostructured materials on biointerfacial interactions. *Advanced Drug Delivery Reviews* **2012,** *64* (15), 1820-1839.
175. Dutta, D.; Sundaram, S. K.; Teeguarden, J. G.; Riley, B. J.; Fifield, L. S.; Jacobs, J. M.; Addleman, S. R.; Kaysen, G. A.; Moudgil, B. M.; Weber, T. J., Adsorbed proteins influence the biological activity and molecular targeting of nanomaterials. *Toxicological Sciences* **2007,** *100* (1), 303-315.
176. Chakraborty, S.; Joshi, P.; Shanker, V.; Ansari, Z.; Singh, S. P.; Chakrabarti, P., Contrasting effect of gold nanoparticles and nanorods with different surface modifications on the structure and activity of bovine serum albumin. *Langmuir* **2011,** *27* (12), 7722-7731.
177. Andersen, A. J.; Hashemi, S. H.; Andresen, T. L.; Hunter, A. C.; Moghimi, S. M., Complement: alive and kicking nanomedicines. *Journal of biomedical nanotechnology* **2009,** *5* (4), 364-372.
178. Pedersen, M. B.; Zhou, X.; Larsen, E. K. U.; Sørensen, U. S.; Kjems, J.; Nygaard, J. V.; Nyengaard, J. R.; Meyer, R. L.; Boesen, T.; Vorup-Jensen, T., Curvature of synthetic and natural surfaces is an important target feature in classical pathway complement activation. *The journal of immunology* **2010,** *184* (4), 1931-1945.
179. Moghimi, S. M.; Andersen, A. J.; Ahmadvand, D.; Wibroe, P. P.; Andresen, T. L.; Hunter, A. C., Material properties in complement activation. *Advanced drug delivery reviews* **2011,** *63* (12), 1000-1007.
180. Janssen, B. J.; Christodoulidou, A.; McCarthy, A.; Lambris, J. D.; Gros, P., Structure of C3b reveals conformational changes that underlie complement activity. *Nature* **2006,** *444* (7116), 213.
181. Chu, K. S.; Hasan, W.; Rawal, S.; Walsh, M. D.; Enlow, E. M.; Luft, J. C.; Bridges, A. S.; Kuijer, J. L.; Napier, M. E.; Zamboni, W. C., Plasma, tumor and tissue pharmacokinetics of Docetaxel delivered via nanoparticles of different sizes and shapes in mice bearing SKOV-3 human ovarian carcinoma xenograft. *Nanomedicine: Nanotechnology, Biology and Medicine* **2013,** *9* (5), 686-693.
182. Arnida, M.; Ray, A.; Peterson, C.; Ghandehari, H., Geometry and surface characteristics of gold nanoparticles influence their biodistribution and uptake by macrophages. *European Journal of Pharmaceutics and Biopharmaceutics* **2011,** *77* (3), 417.
183. Chen, T.; Guo, X.; Liu, X.; Shi, S.; Wang, J.; Shi, C.; Qian, Z.; Zhou, S., A strategy in the design of micellar shape for cancer therapy. *Advanced Healthcare Materials* **2012,** *1* (2), 214-224.

184. Li, W.; Zhang, X.; Hao, X.; Jie, J.; Tian, B.; Zhang, X., Shape design of high drug payload nanoparticles for more effective cancer therapy. *Chemical Communications* **2013,** *49* (93), 10989-10991.
185. Van De Ven, A. L.; Kim, P.; Fakhoury, J. R.; Adriani, G.; Schmulen, J.; Moloney, P.; Hussain, F.; Ferrari, M.; Liu, X.; Yun, S.-H., Rapid tumoritropic accumulation of systemically injected plateloid particles and their biodistribution. *Journal of Controlled Release* **2012,** *158* (1), 148-155.
186. Jasinski, D. L.; Li, H.; Guo, P., The effect of size and shape of RNA nanoparticles on biodistribution. *Molecular Therapy* **2018,** *26* (3), 784-792.
187. Yin, Y.; Hao, Y.; Wang, N.; Yang, P.; Li, N.; Zhang, X.; Song, Y.; Feng, X.; Ma, W., PPy nanoneedle based nanoplatform capable of overcoming biological barriers for synergistic chemo-photothermal therapy. *RSC Advances* **2020,** *10* (13), 7771-7779.
188. Hui, Y.; Wibowo, D.; Liu, Y.; Ran, R.; Wang, H.-F.; Seth, A.; Middelberg, A. P.; Zhao, C.-X., Understanding the effects of nanocapsular mechanical property on passive and active tumor targeting. *ACS nano* **2018,** *12* (3), 2846-2857.
189. Kolhar, P.; Anselmo, A. C.; Gupta, V.; Pant, K.; Prabhakarpandian, B.; Ruoslahti, E.; Mitragotri, S., Using shape effects to target antibody-coated nanoparticles to lung and brain endothelium. *Proceedings of the National Academy of Sciences* **2013,** *110* (26), 10753-10758.
190. Toy, R.; Hayden, E.; Shoup, C.; Baskaran, H.; Karathanasis, E., The effects of particle size, density and shape on margination of nanoparticles in microcirculation. *Nanotechnology* **2011,** *22* (11), 115101.
191. Lee, S.-Y.; Ferrari, M.; Decuzzi, P., Shaping nano-/micro-particles for enhanced vascular interaction in laminar flows. *Nanotechnology* **2009,** *20* (49), 495101.
192. Ta, H. T.; Truong, N. P.; Whittaker, A. K.; Davis, T. P.; Peter, K., The effects of particle size, shape, density and flow characteristics on particle margination to vascular walls in cardiovascular diseases. *Expert opinion on drug delivery* **2018,** *15* (1), 33-45.
193. Cooley, M.; Sarode, A.; Hoore, M.; Fedosov, D. A.; Mitragotri, S.; Gupta, A. S., Influence of particle size and shape on their margination and wall-adhesion: implications in drug delivery vehicle design across nano-to-micro scale. *Nanoscale* **2018,** *10* (32), 15350-15364.
194. Da Silva-Candal, A.; Brown, T.; Krishnan, V.; Lopez-Loureiro, I.; Ávila-Gómez, P.; Pusuluri, A.; Pérez-Díaz, A.; Correa-Paz, C.; Hervella, P.; Castillo, J., Shape effect in active targeting of nanoparticles to inflamed cerebral endothelium under static and flow conditions. *Journal of Controlled Release* **2019,** *309*, 94-105.
195. Jurney, P.; Agarwal, R.; Singh, V.; Choi, D.; Roy, K.; Sreenivasan, S.; Shi, L., Unique size and shape-dependent uptake behaviors of non-spherical nanoparticles by endothelial cells due to a shearing flow. *Journal of Controlled Release* **2017,** *245*, 170-176.
196. Zhu, X.; Vo, C.; Taylor, M.; Smith, B. R., Non-spherical micro-and nanoparticles in nanomedicine. *Materials Horizons* **2019,** *6*, 1094-1121.
197. Myerson, J. W.; Anselmo, A. C.; Liu, Y.; Mitragotri, S.; Eckmann, D. M.; Muzykantov, V. R., Non-affinity factors modulating vascular targeting of nano-and microcarriers. *Advanced drug delivery reviews* **2016,** *99*, 97-112.
198. Smith, B. R.; Kempen, P.; Bouley, D.; Xu, A.; Liu, Z.; Melosh, N.; Dai, H.; Sinclair, R.; Gambhir, S. S., Shape matters: intravital microscopy reveals surprising geometrical dependence for nanoparticles in tumor models of extravasation. *Nano Letters* **2012,** *12* (7), 3369-3377.
199. Chauhan, V. P.; Popović, Z.; Chen, O.; Cui, J.; Fukumura, D.; Bawendi, M. G.; Jain, R. K., Fluorescent nanorods and nanospheres for real-time in vivo probing of nanoparticle shape-dependent tumor penetration. *Angewandte Chemie* **2011,** *123* (48), 11619-11622.
200. Godin, B.; Chiappini, C.; Srinivasan, S.; Alexander, J. F.; Yokoi, K.; Ferrari, M.; Decuzzi, P.; Liu, X., Discoidal porous silicon particles: fabrication and biodistribution in breast cancer bearing mice. *Advanced functional materials* **2012,** *22* (20), 4225-4235.
201. Sun, Q.; Ojha, T.; Kiessling, F.; Lammers, T.; Shi, Y., Enhancing tumor penetration of nanomedicines. *Biomacromolecules* **2017,** *18* (5), 1449-1459.

202. Huang, X.; Li, L.; Liu, T.; Hao, N.; Liu, H.; Chen, D.; Tang, F., The shape effect of mesoporous silica nanoparticles on biodistribution, clearance, and biocompatibility in vivo. *ACS nano* **2011,** *5* (7), 5390-5399.
203. Christian, D. A.; Cai, S.; Garbuzenko, O. B.; Harada, T.; Zajac, A. L.; Minko, T.; Discher, D. E., Flexible filaments for in vivo imaging and delivery: persistent circulation of filomicelles opens the dosage window for sustained tumor shrinkage. *Molecular pharmaceutics* **2009,** *6* (5), 1343-1352.
204. Shukla, S.; Eber, F. J.; Nagarajan, A. S.; DiFranco, N. A.; Schmidt, N.; Wen, A. M.; Eiben, S.; Twyman, R. M.; Wege, C.; Steinmetz, N. F., The impact of aspect ratio on the biodistribution and tumor homing of rigid soft-matter nanorods. *Advanced healthcare materials* **2015,** *4* (6), 874-882.
205. Bruckman, M. A.; Randolph, L. N.; VanMeter, A.; Hern, S.; Shoffstall, A. J.; Taurog, R. E.; Steinmetz, N. F., Biodistribution, pharmacokinetics, and blood compatibility of native and PEGylated tobacco mosaic virus nano-rods and-spheres in mice. *Virology* **2014,** *449*, 163-173.
206. Kaga, S.; Truong, N. P.; Esser, L.; Senyschyn, D.; Sanyal, A.; Sanyal, R.; Quinn, J. F.; Davis, T. P.; Kaminskas, L. M.; Whittaker, M. R., Influence of size and shape on the biodistribution of nanoparticles prepared by polymerization-induced self-assembly. *Biomacromolecules* **2017,** *18* (12), 3963-3970.
207. Fu, X.; Cai, J.; Zhang, X.; Li, W.-D.; Ge, H.; Hu, Y., Top-down fabrication of shape-controlled, monodisperse nanoparticles for biomedical applications. *Advanced Drug Delivery Reviews* **2018**.
208. Maeki, M.; Kimura, N.; Sato, Y.; Harashima, H.; Tokeshi, M., Advances in microfluidics for lipid nanoparticles and extracellular vesicles and applications in drug delivery systems. *Advanced Drug Delivery Reviews* **2018,** *128*, 84-100.
209. Mai, Y.; Eisenberg, A., Self-assembly of block copolymers. *Chemical Society Reviews* **2012,** *41* (18), 5969-5985.
210. Cauchois, O.; Segura-Sanchez, F.; Ponchel, G., Molecular weight controls the elongation of oblate-shaped degradable poly (γ-benzyl-L-glutamate) nanoparticles. *International Journal of Pharmaceutics* **2013,** *452* (1-2), 292-299.
211. Yoo, J.-W.; Chambers, E.; Mitragotri, S., Factors that control the circulation time of nanoparticles in blood: challenges, solutions and future prospects. *Current Pharmaceutical Design* **2010,** *16* (21), 2298-2307.
212. Pulskamp, K.; Diabaté, S.; Krug, H. F., Carbon nanotubes show no sign of acute toxicity but induce intracellular reactive oxygen species in dependence on contaminants. *Toxicology letters* **2007,** *168* (1), 58-74.
213. Murphy, C. J.; Gole, A. M.; Stone, J. W.; Sisco, P. N.; Alkilany, A. M.; Goldsmith, E. C.; Baxter, S. C., Gold nanoparticles in biology: beyond toxicity to cellular imaging. *Accounts of chemical research* **2008,** *41* (12), 1721-1730.
214. Alkilany, A. M.; Murphy, C. J., Toxicity and cellular uptake of gold nanoparticles: what we have learned so far? *Journal of nanoparticle research* **2010,** *12* (7), 2313-2333.

8. Abbreviations

AFM: Atomic force microscopy

AR: aspect ratio

Au: gold

CARPA: complement activation-related pseudoallergy

CLSM: Confocal laser scanning microscopy.

CTAB: Cetyl trimethylammonium bromide

DOPE: dioleoylphosphatidylethanolamine

DOTAP: 1,2-dioleoyl-3-trimethylammoniumpropane

ICAM-1: intracellular adhesion molecule

IPC-AES: Inductively coupled plasma-atomic emission spectrometer

M&NPs: micro- and nanoparticles

MPS: mononuclear phagocytic system

PEG: polyethylene glycol

PGS: poly(glycerol sebacate)

PISA: polymerization-induced self-assembly

PLGA: poly(lactic acid)-*co*-(glycolic acid)

PRINT: Particle Replication In Nonwetting Templates

ROS: reactive oxygen species

SWNTs: single-walled carbon nanotubes

TEM: Transmission electron microscopy.